Secrecy of Multi-Antenna Transmission With Full-Duplex User in the Presence of Randomly Located Eavesdroppers

Ishmam Zabir, *Graduate Student Member, IEEE*, Ahmed Maksud, *Student Member, IEEE*, Gaojie Chen, *Senior Member, IEEE*, Brian M. Sadler, *Life Fellow, IEEE*, and Yingbo Hua, *Fellow, IEEE*

***Abstract*— This paper considers the secrecy performance of several schemes for multi-antenna transmission to single-antenna users with full-duplex (FD) capability against randomly distributed single-antenna eavesdroppers (EDs). These schemes and related scenarios include transmit antenna selection (TAS), transmit antenna beamforming (TAB), artificial noise (AN) from the transmitter, user selection based their distances to the transmitter, and colluding and non-colluding EDs. The locations of randomly distributed EDs and users are assumed to be distributed as Poisson Point Process (PPP). We derive closed form expressions for the secrecy outage probabilities (SOP) of all these schemes and scenarios. The derived expressions are useful to reveal the impacts of various environmental parameters and user's choices on the SOP, and hence useful for network design purposes. Examples of such numerical results are discussed.**

***Index Terms*— Physical layer security, beamforming, artificial noise, stochastic geometry, full duplex, secrecy connectivity, power allocation.**

I. Introduction

SINCE Wyner's work [1], physical layer security has been studied as an alternative or complementary approach to cryptography for information security. This trend of study has accelerated in recent years given its importance for 5G and future wireless networks [2].

Due to the broadcast nature of wireless communications, transmitted information in air is highly vulnerable to eavesdropping unless a positive secrecy rate at the physical layer is achieved. Many prior works for achieving a positive secrecy rate require that the locations and/or channel-state-information (CSI) of eavesdroppers (EDs or Eve) are known to the legitimate users (also referred to as users) [3]–[12]. This requirement is generally difficult to meet in practice.

Manuscript received June 27, 2020; revised September 18, 2020 and December 3, 2020; accepted December 11, 2020. Date of publication December 28, 2020; date of current version February 1, 2021. This work was supported in part by the Army Research Office under Grant W911NF-17-1-0581. The associate editor coordinating the review of this manuscript and approving it for publication was Dr. Ragnar Thobaben. *(Corresponding author: Yingbo Hua.)*

Ishmam Zabir, Ahmed Maksud, and Yingbo Hua are with Department of Electrical and Computer Engineering, University of California, Riverside, CA 92521 USA (e-mail: izabi001@ucr.edu; amaks002@ucr.edu; yhua@ee.ucr.edu).

Gaojie Chen is with the School of Engineering, University of Leicester, Leicester LE1 7RH, U.K. (e-mail: gaojie.chen@leicester.ac.uk).

Brian M. Sadler is with the Army Research Laboratory, Adelphi, MD 20783 USA (e-mail: brian.sadler@ieee.org).

Digital Object Identifier 10.1109/TIFS.2020.3047763

One way to handle EDs whose locations and CSI are unknown to users is to assume a statistical model for EDs' CSI where both the small-scale-fading and large-scale-fading of EDs' CSI are statistically modelled. While the small-scale-fading is commonly modelled as Gaussian distributed, the large-scale-fading can be treated by assuming EDs to be randomly distributed according to a Poisson Point Process (PPP) [13]–[24]. This paper will also adopt the PPP model to investigate the impact of random EDs locations on secrecy performance which is useful over a time window within which the EDs' locations change randomly.

The conventional radio is half-duplex (HD). But full-duplex (FD) radio promises to be available in the near future [25]–[30]. A user equipped with FD capability can receive a desired information while transmitting an artificial noise (AN) to jam nearby EDs [7], [27]–[31]. We will also refer to this AN as Rx-AN which differs from the AN (along with information signal) transmitted by a multi-antenna transmitter. The latter will also be referred to as Tx-AN. Subject to randomly distributed EDs, schemes based on Tx-AN without Rx-AN have been studied in [16]–[20] for non-colluding EDs and in [21]–[24] for colluding EDs. In [16], authors investigated the design of multi-antenna Tx-AN to minimize the secrecy outage probability (SOP) by ignoring thermal noise at EDs. In [17] and [18], authors derived exact closed-form expressions for optimal Tx-AN allocation to minimize SOP. In [19], authors further investigated secrecy performance under imperfect CSI. The aforementioned studies reveal that Tx-AN (for HD receiver) improves secrecy performance against any EDs' scenarios.

This paper will present statistical analyses of SOP for a range of downlink transmission schemes for pairs of multi-antenna base-station (BS) and single-antenna user equipment (UE) in the presence of randomly located EDs, which is illustrated in Fig. 1. These schemes include the following scenarios: the BS may or may not apply Tx-AN, the UE may or may not apply Rx-AN or equivalently operate in either FD or HD mode, and the EDs may or may not collude with each other to form a virtual antenna array. For randomly distributed UEs, the BS can have them ordered according to their distances to the BS before a downlink transmission may be applied. Furthermore, the BS may apply a transmit-antenna-selection (TAS) scheme or a transmit-antenna-beamforming (TAB) scheme. The TAB scheme requires full CSI knowledge at BS whereas the TAS scheme is a comparatively low-cost low-complexity method [32]. In particular, we will focus on the SOP for all the schemes listed above (with exception shown in Table I). The organization of these analyses is shown

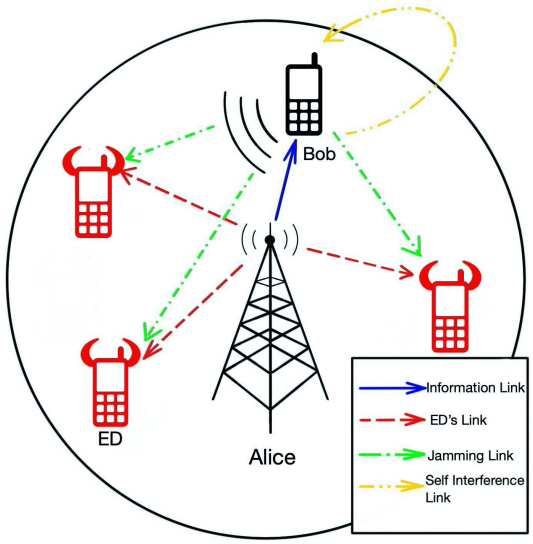

Fig. 1. Wireless network subject to randomly located eavesdroppers where Alice is BS and UE is Bob.

TABLE I
ORGANIZATION OF SECTIONS III AND IV

	non-colluding EDs			colluding EDs	
	FD UE	HD UE	multi-UE ordering	FD UE	HD UE
TAS	III-A	III-A1	[35]	IV-A	IV-B
TAB	III-B	III-B2	III-C	IV-C& IV-D	IV-C1

in Table I. Note that HD is a special case of FD, and using no Tx-AN is a special case of using Tx-AN. Much of the mathematical details is given in appendices. Section V shows numerical results to verify the analysis. Section IX summarizes the paper.

The key contributions of this paper (a substantial extension of [34]) include the following:

- We derive the closed form expressions of SOP for all the schemes/scenarios listed in Table I. In the context of randomly distributed EDs, the scheme with both Tx-AN and Rx-AN was not studied before, and none of the schemes listed under colluding EDs was before considered either.
- We focus on SOP conditional on user's CSI, which results in a tight lower bound of SOP for both TAS and TAB schemes against randomly located colluding EDs. This is in contrast to [33] where TAS was analyzed based on unconditional SOP and zero thermal noise at EDs. The latter is only valid for scenarios of high jamming noise.
- We extend the analysis shown in [35] from TAS to TAB with Tx-AN for multiple HD users. Comparisons between TAS and TAB are shown analytically and numerically. (The low cost advantage of antenna selection has been exploited for network throughput as well as physical layer security [44]–[47]. But TAS shown in [33] and [35] is the most relevant to this paper.)
- We reveal the existence of a finite optimum Rx-AN power for both TAS and TAB schemes, which can be also computed based on our closed form SOP expressions.

The symbols used in this paper are shown in Table II.

TABLE II
NOTATION AND SYMBOLS

Symbol	Definition
$\mathcal{CN}$	complex Gaussian
Φ	the set of locations of EDs
ρ_E	intensity or density of Φ
α	path loss exponent
ρ	normalized self-interference coefficient
P_T	transmission (signal plus AN) power from Alice
P_J	transmission (jamming) power from Bob
ϵ	fraction of transmission power at Alice for AN
$\mathbb{E}_{\mathbf{v}}$	expectation over v
$[x]^+$	max(0,x)
$B(x,y)$	Beta function, where $B(x,y)=\frac{\Gamma(x)\Gamma(y)}{\Gamma(x+y)}$
$\Gamma(x,y)$	upper incomplete Gamma function
$\gamma(x,y)$	lower incomplete Gamma function
$U(a,b,z)$	Confluent hypergeometric function of second kind
$\mathbf{F}(a,b,c;z)$	Gaussian hypergeometric function
$\mathcal{L}$	Laplace transform
$\mathbf{E_1}(x)$	Exponential integral function

II. System Model

We consider a base station (BS or Alice) with multiple antennas located at the center of a circle of radius R, which transmits secret information to a single-antenna (omnidirectional) user equipment (UE or Bob). Without loss of generality, we first assume that Bob is located at a unit distance away from Alice. There are randomly located single-antenna (omnidirectional) eavesdroppers (EDs) in the circle, and the random locations of EDs (denoted by Φ) are modeled as a PPP with the intensity ρ_E.

The channel gain vector from Alice to Bob is denoted by $\mathbf{h} \in \mathcal{C}^{M\times 1}$, which has been normalized to be a complex Gaussian random vector with zero mean and the identity covariance matrix, i.e., $\mathcal{CN}(\mathbf{0},\mathbf{I})$. We assume Bob is equipped with full-duplex antenna (full-duplex can be implemented with either one Tx and one Rx antenna or even with single antenna via RF circulator [36]) where Bob can transmit and receive at the same time in the same frequency band. The normalized residual instantaneous self-interference channel gain at Bob is $\sqrt{\rho}g_B$ with the distribution $\mathcal{CN}(0,\rho)$ where ρ corresponds to a normalized gain factor (which is relative to the main/user channel gain and should be kept small in application although it can be larger than one if the actual distance between Alice and Bob is relatively large [29]). The channel vector from Alice to the eth ED is $\sqrt{a_e}\mathbf{h}_{AE_e} \in \mathcal{C}^{M\times 1}$ and distributed as $\mathcal{CN}(\mathbf{0}, a_e\mathbf{I})$, and the channel gain from Bob to the eth ED is $\sqrt{b_e}h_{BE_e}$ and distributed as $\mathcal{CN}(0,b_e)$. We also let $a_e=\frac{1}{d^{\alpha}_{AE_e}}$ with d_{AE_e} being the normalized distance between Alice and the eth ED, and $b_e=\frac{1}{d^{\alpha}_{BE_e}}$ with d_{BE_e} being the normalized distance between Bob and the eth ED. Note that a_e and b_e are the large-scale fading parameters as they are dependent on the location of ED while $\mathbf{h}$, g_B, $\mathbf{h}_{AE_e}$ and h_{BE_e} are the small-scale fading parameters. We assume that the channels are all quasi-static where the channel coefficients stay constant during transmission of any given packet.

The secrecy rate of the downlink transmission from Alice to Bob is

$$S_{AB}=[\log_2(1+SNR_{AB})-\log_2(1+SNR_{AE_*})]^+, \quad (1)$$

where $SNR_{AE_*}=\mathcal{F}(SNR_{AEe})$. The operator $\mathcal{F}(.)$ takes the location dependent Signal-to-Noise Ratios (SNRs) of EDs as argument. The form of $\mathcal{F}(.)$ is dependent on whether EDs are acting independently or colluding with each other. In the case of non-colluding EDs, the strongest ED channel is considered

and the form of $\mathcal{F}(.)$ is defined as

$$\mathcal{F}(.) = \max_{e\in\Phi}(.). \tag{2}$$

In the case of colluding EDs, we assume that all EDs can combine their own SNRs to jointly decode the information bearing signal. We consider passive (distributed) EDs. Since they do not have access to the full CSI between Alice and themselves, they are unable to form a virtual antenna array for colluding. This assumption is the same as in [13]–[15], [24] and [33]–[35]. Thus,

$$\mathcal{F}(.) = \sum_{e\in\Phi}(.). \tag{3}$$

For a target secrecy rate R_S, the SOP is defined as

$$P_{out} \triangleq P(S_{AB} \le R_S) = P\left[\frac{1+SNR_{AB}}{1+SNR_{AE_*}} \le 2^{R_S}\right], \tag{4}$$

where $P(\cdot)$ denotes the probability. We will also use $P_{con} \triangleq 1 - P_{out}$.

A. Transmit Antenna Selection

In the TAS scheme, Alice only transmits via the antenna corresponding to the element in $\mathbf{h}$ that has the largest amplitude. Let $\sqrt{P_T}x_A(k)$ of power P_T be the information signal transmitted from Alice, and h_{i^*} be the element selected from $\mathbf{h} = [h_1, \cdots, h_M]^T$, i.e., $|h_{i^*}| = \max_i |h_i|$. Thus, Bob and Eve receive the following signals respectively:

$$y_B(k) = h_{i^*}\sqrt{P_T}x_A(k) + \sqrt{\rho P_J}g_B\tilde{w}_B(k) + n_B(k), \tag{5}$$

$$y_{E_e}(k) = \sqrt{a_e P_T}h_{A_{i^*}E_e}x_A(k) + \sqrt{b_e P_J}h_{BE_e}w_B(k) + n_{E_e}(k), \tag{6}$$

where $\sqrt{P_J}w_B(k)$ of power P_J is the jamming noise or Rx-AN from Bob, $n_B(k)$ and $n_E(k)$ are the background Gaussian noises at Bob and Eve each with the unit variance, and the second term of (5) denotes the residual self-interference. Then, the SNR at Bob is

$$SNR_{AB}^{TAS} = \frac{|h_{i^*}|^2 P_T}{1+\rho|g_B|^2 P_J}, \tag{7}$$

and the SNR at the eth Eve is

$$SNR_{AEe}^{TAS} = \frac{a_e|h_{A_{i^*}E_e}|^2 P_T}{1+b_e|h_{BE_e}|^2 P_J}. \tag{8}$$

B. Transmit Antenna Beamforming

In the TAB scheme, Alice takes the advantage of the complete knowledge of $\mathbf{h}$ by transmitting the following signal:

$$\mathbf{s}(k) = \sqrt{(1-\epsilon)P_T}\mathbf{t}x_A(k) + \sqrt{\frac{\epsilon P_T}{M-1}}\mathbf{W}\mathbf{v}(k), \tag{9}$$

where $x_A(k)$ is the message signal of zero mean and unit variance, $\mathbf{t} = \frac{\mathbf{h}^*}{\|\mathbf{h}\|}$, $\mathbf{W} \in \mathcal{C}^{M\times(M-1)}$ has the orthonormal columns that span the left null space of $\mathbf{t}$ (hence $\mathbf{t}\mathbf{t}^H + \mathbf{W}\mathbf{W}^H = \mathbf{I}$), $\mathbf{v} \in \mathcal{C}^{(M-1)\times 1}$ is the Tx-AN $\mathcal{CN}(\mathbf{0}, \mathbf{I})$, and $\epsilon \in \{0, 1\}$ is the power fraction factor that splits the total power P_T between the Tx-AN term and the message term.

Consequently, the received signal at Bob and the eth Eve are:

$$y_B(k) = \sqrt{(1-\epsilon)P_T}\|\mathbf{h}\|x_A(k) + \sqrt{\rho P_J}g_B\tilde{w}_B(k) + n_B(k),$$

$$y_{E_e}(k) = \sqrt{a_e(1-\epsilon)P_T}\frac{\mathbf{h}_{AEe}^T\mathbf{h}^*}{\|\mathbf{h}\|}x_A(k) + \sqrt{b_e P_J}h_{BE_e}w_B(k) + \sqrt{a_e}\sqrt{\frac{\epsilon P_T}{M-1}}\mathbf{h}_{AEe}^T\mathbf{W}\mathbf{v}(k) + n_{E_e}(k),$$

respectively. Then the SNR at Bob is

$$SNR_{AB}^{TAB} = \frac{(1-\epsilon)\|\mathbf{h}\|^2 P_T}{1+\rho|g_B|^2 P_J}, \tag{10}$$

and the SNR at the eth Eve is

$$\begin{aligned} SNR_{AE_e}^{TAB} &= \frac{a_e(1-\epsilon)\frac{|\mathbf{h}_{AE_e}^T\mathbf{h}^*|^2}{\|\mathbf{h}\|^2}P_T}{1+b_e|h_{BE_e}|^2P_J + a_e\frac{\epsilon P_T}{M-1}\mathbb{E}_{\mathbf{v}}\{|\mathbf{h}_{AE_e}^T\mathbf{W}\mathbf{v}|^2\}} \\ &= \frac{a_e(1-\epsilon)\frac{|\mathbf{h}_{AE_e}^T\mathbf{h}^*|^2}{\|\mathbf{h}\|^2}P_T}{1+b_e|h_{BE_e}|^2P_J + a_e\frac{\epsilon P_T}{M-1}\|\mathbf{h}_{AE_e}\|^2(1-\frac{|\mathbf{h}_{AE_e}^T\mathbf{h}^*|^2}{\|\mathbf{h}_{AE_e}\|^2\|\mathbf{h}\|^2})} \\ &= \frac{(1-\epsilon)X_1\Theta P_T}{d_{AE_e}^\alpha + \frac{P_J d_{AE_e}^\alpha}{d_{BE_e}^\alpha}X_2 + \frac{\epsilon P_T}{M-1}X_1(1-\Theta)}, \end{aligned} \tag{11}$$

where $\mathbb{E}_{\mathbf{v}}$ denotes the expectation over $\mathbf{v}$ and $\mathbb{E}_{\mathbf{v}}\{|\mathbf{h}_{AE_e}^T\mathbf{W}\mathbf{v}|^2\} = \mathbb{E}_{\mathbf{v}}\{|\mathbf{h}_{AE_e}^T\mathbf{W}\mathbf{v}\mathbf{v}^T\mathbf{W}^T\mathbf{h}_{AE_e}|^2\} = \mathbf{h}_{AE_e}^T(\mathbf{I} - \mathbf{t}\mathbf{t}^H)\mathbf{h}_{AE_e}$, $X_1 = \|\mathbf{h}_{AE_e}\|^2$, $X_2 = |h_{BE_e}|^2$ and $\Theta = \frac{|\mathbf{h}_{AE_e}^T\mathbf{h}^*|^2}{\|\mathbf{h}_{AE_e}\|^2\|\mathbf{h}\|^2}$. Note that X_1, X_2 and Θ are independent of each other.

Furthermore, X_1 has a Chi-squared distribution with $2M$ degrees of freedom (DoF), i.e., its probability density function (PDF) is $f_{X_1}(x) = \frac{x^{M-1}e^{-x}}{\Gamma(M)}$; X_2 has a Chi-squared distribution with 2 DoF (also known as the exponential distribution of the unit mean); and Θ is known to have the beta distribution [30] with parameters $B(1, M-1)$, i.e., $f_\Theta(x) = (M-1)(1-x)^{M-2}$. Note that $Beta(a, b)$ distributed random variable X the PDF $f_X(x) = \frac{x^{a-1}(1-x)^{b-1}}{B(a,b)}$.

In order to maintain a data rate R_D from Alice to Bob, we must have $\log_2(1 + SNR_{AB}^{TAB}) > R_D$, i.e., $1 - \epsilon > \frac{1+\rho|g_B|^2P_J}{\|\mathbf{h}\|^2P_T}(2^{R_D} - 1)$ for the non-negative ϵ.

C. TAB With User Selection (TAB-US)

In the TAB-US scheme, we assume that Alice (BS) serves multiple single-antenna HD Bobs (UEs) (where $P_J = 0$) based on the user's distance from Alice. The locations of Eves and Bobs are all modeled as spatial PPP, i.e., Φ_E with intensity ρ_E and Φ_U with intensity ρ_U respectively.

Let d_{AB_n} be the distance from Alice to the nth (nearest) Bob. Similar to (10), the SNR at the nth Bob is

$$SNR_{AB_n} = \frac{(1-\epsilon)P_T\|\mathbf{h}_{AB_n}\|^2}{d_{AB_n}^\alpha}, \tag{12}$$

and, similar to (11), the SNR at the eth Eve is

$$SNR_{AE_e} = \frac{a_e(1-\epsilon)\|\mathbf{h}_{AE_e}\|^2\frac{\|\mathbf{h}_{AE_e}^H\mathbf{h}_{AB_n}\|^2}{\|\mathbf{h}_{AE_e}\|^2\|\mathbf{h}_{AB_n}\|^2}P_T}{1+a_e\frac{\epsilon P_T}{M-1}\|\mathbf{h}_{AE_e}\|^2(1-\frac{\|\mathbf{h}_{AE_e}^H\mathbf{h}_{AB_n}\|^2}{\|\mathbf{h}_{AE_e}\|^2\|\mathbf{h}_{AB_n}\|^2})}, \tag{13}$$

where $X_{2,n} = \|\mathbf{h}_{AB_n}\|^2$ is independent from X_1 and both follow the Chi-squared distribution with $2M$ degrees of freedom, i.e., $f_{X_{2,n}}(x) = f_{X_1}(x) = \frac{x^{M-1}e^{-x}}{\Gamma(M)}$. Also $\Theta = \frac{\|\mathbf{h}_{AE_e}^H \mathbf{h}_{AB_n}\|^2}{\|\mathbf{h}_{AE_e}\|^2 \|\mathbf{h}_{AB_n}\|^2}$ follows the $B(1, M-1)$ distribution [30], and $X_4 = \Theta X_1$ is exponentially distributed with mean equal to one. Also, $X_{4,4} = (1-\Theta)X_1$ follows $\Gamma(M-1, 1)$ distribution and most importantly $X_{2,n}$, X_4 and $X_{4,4}$ are independent.

III. Secrecy Performance Against Non-Colluding Eavesdroppers

Throughout this section, we study the secrecy performance of both the TAB and TAS schemes against independently acting EDs.

Furthermore, we analyze the secrecy performance of the TAB scheme as a function of the ordering index of each Bob (among randomly distributed Bobs) with respect to his distance to Alice.

A. Secrecy Performance of the TAS Scheme

The performance of the TAS scheme was analyzed in [33] by assuming that the noise at each node is dominated by the interference. A novelty of the following analysis is an insight that there is generally a nonzero optimal P_J. Such an analytical insight would not be possible if the noise is assumed to be negligible from the very beginning of the analysis. Moreover, authors of [33] derived the SOP expression averaged over the distribution of legitimate channel. Such analysis does not provide useful insights for a given/common realization of the legitimate channel. In this paper, we study the SOP expression conditioned on the legitimate channel CSI. For a large coherence period of the legitimate channel, the SOP averaged over EDs' distribution can be minimized over the jamming power from FD Bob. Thus, this study enables us to find the optimum allocation at Bob. We will also show the overall averaged SOP considering the distribution of the legitimate channel.

We will use the following parameterizations: $\beta \triangleq 2^{R_s}$, $m \triangleq \frac{P_J}{P_T}$ ("a transmit power ratio"), $Y \triangleq SNR_{AB}^{TAS} = \frac{|h_{i^*}|^2}{\frac{1}{P_T}+\rho m|g_B|^2}$ and $Y_0 \triangleq \frac{Y}{\beta}+\frac{1}{\beta}-1$. Note that for any given realization of $\mathbf{h}$ and g_B, Y is a given constant. Hence, $P[S_{AB}^{TAS} > R_s|\Phi, \mathbf{h}, g_B] = P[S_{AB}^{TAS} > R_s|\Phi, Y]$.

Proposition 1: Conditioned on $\mathbf{h}$ and g_B, the probability of achieving a secrecy rate strictly larger than R_s using the TAS scheme is given by

$$P_{con,Y} = \exp\left[-\rho_E \int_0^R \int_0^{2\pi} \Psi(Y, r, \theta) r \mathrm{d}\theta \mathrm{d}r \right], \quad (14)$$

where

$$\Psi(Y, r_e, \theta_e) = \frac{\exp(-\frac{d_{AE_e}^{\alpha}}{P_T} Y_0)}{1 + m(\frac{d_{AE_e}}{d_{BE_e}})^{\alpha} Y_0}, \quad (15)$$

and (r_e, θ_e) are the polar coordinates of the location of the eth Eve with the origin at the location of Alice. Also $d_{AE_e} = r_e$ and $d_{BE_e} = \sqrt{r_e^2 + d^2 - 2r_e \cos\theta}$.
The proof is shown in Appendix A.

Remark 1: It is obvious that $P_{con,Y}$ is a decreasing function of $\Psi(Y, r, \theta)$. One can verify the following statements subject to $P_T > 0$:

TABLE III

Effects of Parameters on $\Psi(Y, r, \theta)$ & $P_{con,Y}$ When $R_s = 0$, Where $-$, $\uparrow$ and $\downarrow$ Denote Invariance, Increasing and Decreasing, Respectively

	P_T	$P_J \to \infty (\rho P_J = a)$	$P_J \uparrow (\leq P_J{}^*)$	$P_J \uparrow (\geq P_J{}^*)$
$\Psi(Y, r, \theta)$	$-$	$\to 0$	$\downarrow$	$\uparrow$
$P_{con,Y}$	$-$	$\to 1$	$\uparrow$	$\downarrow$

- If $R_s = 0$, then $\Psi(Y, r, \theta)$ is invariant to P_T.
- If $R_s = 0$ and the product ρP_J is a fixed constant, then as P_J increases to ∞, $\Psi(Y, r, \theta)$ decreases monotonically to zero and hence $P_{con,Y}$ increases monotonically to one.
- If $\rho \ll 1$, then in a region of small P_J, Y and hence Y_0 are approximately invariant to P_J. But in this case, $\Psi(Y, r, \theta)$ decreases as P_J increases (since $Y_0 \left(\frac{d_{AE}}{d_{BE}}\right)^{\alpha}$ is not small) and hence $P_{con,Y}$ increases as P_J increases.

The aforementioned statements are summarized in Table III where $P_J{}^*$ is nonzero optimal value of P_J and a is an arbitrary constant. Here $P_J \to \infty$ implies that the jamming power from Bob is large or more precisely $P_J \gg \frac{1}{\rho|g_B|^2}$. The expression (14) provides the relationship between the target secrecy rate R_s and different parameters in the network. To obtain $P_{con,Y}$ numerically, the double integrals shown there need to be computed for a given choice of the path loss exponent α. In general, experimentally estimated α results in difficulty for simplification of the double integrals. But for $R_s = 0$ (i.e. $Y_0 = Y$) and $\alpha = 2$, a simplification can be shown to be

$$P_{con,Y} = \exp\Bigg[-\rho_E \Bigg(\frac{\pi P_T}{Y}\left(1 - \exp(-\frac{Y R^2}{P_T})\right) - \pi m Y \times \int_0^{R^2} \frac{\exp(-\frac{Yr}{P_T}) r}{\sqrt{\left((1+mY)r + d^2\right)^2 - 4rd^2}} \mathrm{d}r \Bigg) \Bigg] \quad (16)$$

which is shown in Appendix B.

Then, the unconditional $P_{con} = \mathbb{E}_Y[P_{con,Y}]$ can be obtained by

$$P_{con} = P[S_{AB}^{TAS} > R_s] = \int_{y=0}^{\infty} P_{con,y} f_Y(y) \mathrm{d}y, \quad (17)$$

where the distribution of Y due to the random $|h_{i^*}|^2$ and $|g_B|^2$ is given in the following lemma:

Lemma 1: The cumulative distribution function (CDF) of Y is

$$F_Y(y) = \sum_{i=0}^{M} C_i^M (-1)^i \frac{e^{-\frac{iy}{P_T}}}{1 + iy\rho m}, \quad (18)$$

where $C_i^M = \frac{M!}{(M-i)!i!}$. Hence the PDF of Y is

$$f_Y(y) = \sum_{i=0}^{M} C_i^M (-1)^{i+1} i e^{-\frac{iy}{P_T}} \frac{(\frac{iy\rho m}{P_T} + \frac{1}{P_T} + \rho m)}{(1 + iy\rho m)^2}. \quad (19)$$

Next, we consider $P_{con,Y}$ in the two special cases: $P_J = 0$ and $P_J \to \infty$.

1) The Case of $P_J = 0$: Now we consider the case of $P_J = 0$ thus $m = 0$ and assume that $P_T \gg \frac{1-\beta}{|h_{i^*}|^2}$ thus $Y_0 \approx \frac{P_T|h_{i^*}|^2}{\beta}$. It follows from

(45) that $\Psi(Y;r,\theta) = \exp(-\frac{d_{AEe}^{\alpha}}{P_T}Y_0) = \exp\left(-r^{\alpha}\frac{|h_{i^*}|^2}{\beta}\right)$. Hence

$$\begin{aligned}\frac{\ln P_{con,Y}}{\rho_E} &= -\int_0^R\int_0^{2\pi}\Psi(Y;r,\theta)r\,\mathrm{d}\theta\mathrm{d}r\\ &= -2\pi\int_0^R\exp\left(-r^{\alpha}\frac{|h_{i^*}|^2}{\beta}\right)r\mathrm{d}r\\ &= -\frac{2\pi\beta^{\frac{2}{\alpha}}}{\alpha(|h_{i^*}|^2)^{\frac{2}{\alpha}}}\int_0^{\frac{R^{\alpha}(|h_{i^*}|^2}{\beta}}\exp(-z)z^{\frac{2}{\alpha}-1}\mathrm{d}z\\ &= -\frac{2\pi\beta^{\frac{2}{\alpha}}}{\alpha(|h_{i^*}|^2)^{\frac{2}{\alpha}}}\gamma\left(\frac{2}{\alpha},\frac{|h_{i^*}|^2R^{\alpha}}{\beta}\right),\end{aligned}\tag{20}$$

where $z = r^{\alpha}\frac{|h_{i^*}|^2}{\beta}$ and $\gamma(x,y) = \int_0^y z^{x-1}e^{-z}\mathrm{d}z$ is the lower incomplete gamma function which increases monotonically with y. From (20), it is clear that $P_{con,Y}$ monotonically decreases as R increases. In particular,

$$\lim_{R\to\infty}\frac{\ln P_{con,Y}}{\rho_E} = -\pi\left(\frac{\beta}{|h_{i^*}|^2}\right)^{\frac{2}{\alpha}}\frac{2}{\alpha}\Gamma\left(\frac{2}{\alpha}\right),\tag{21}$$

where $\Gamma(x) = \int_0^{\infty}z^{x-1}e^{-z}\mathrm{d}z$. It is known that $x\Gamma(x) = \Gamma(x+1)$ for positive x and $\Gamma(x+1)$ decreases to one as x decreases to zero. Then, provided $\frac{\beta}{|h_{i^*}|^2} > 1$, the above limit increases as α increases. The result (21) serves as a benchmark corresponding to a HD Bob.

2) The Case of $P_J = \infty$: We now consider the case of $P_J = \infty$ and also assume $R_s = 0$ and $\alpha = 2$. In this case, $Y_0 = Y = 0$ and $mY = \frac{|h_{i^*}|^2}{\rho|g_B|^2}$. Then, following a similar derivation as that in section I of the supplement, one can verify that

$$\begin{aligned}\frac{\ln P_{con,Y}}{\rho_E} = -2\pi\int_{r=0}^R\Bigg(1 &- \frac{1}{\sqrt{1+\rho\frac{|g_B|^2}{|h_{i^*}|^2}(1+\frac{d}{r})^2}}\\ &\times\frac{1}{\sqrt{1+\rho\frac{|g_B|^2}{|h_{i^*}|^2}(1-\frac{d}{r})^2}}\Bigg)r\mathrm{d}r,\end{aligned}\tag{22}$$

where the integrant converges to $\left(1-\frac{1}{1+\rho\frac{|g_B|^2}{|h_{i^*}|^2}}\right)r$ as r becomes large and the integral goes to ∞ as $R\to\infty$. Hence $\lim_{R\to\infty}P_{con,Y} = 0$. This result suggests that P_J should not be too large. Combining this with a previous result for small P_J implies that there is generally a finite nonzero optimal P_J.

B. Secrecy Performance of the TAB Scheme

Unlike the TAS scheme, Alice will now use all transmit antennas via beamforming to transmit each information symbol. We will assume that all the channel links from Alice to Bob are independent and identically distributed.

In addition to $m = \frac{P_J}{P_T}$ and $\beta = 2^{R_s}$, we will use $Z = \frac{SNR_{AB}^{TAB}}{(1-\epsilon)} = \frac{\|\mathbf{h}\|^2}{\frac{1}{P_T}+\rho m|g_B|^2}$, $C = \frac{Z}{\beta P_T} - \frac{(1-\frac{1}{\beta})}{(1-\epsilon)P_T}$, $f_e = (\frac{d_{AEe}}{d_{BEe}})^{\alpha}m$ ("a large scale receive power ratio") and $G = \frac{1}{CP_T} = \frac{\beta(1+\rho P_J|g_B|^2)}{P_T\|\mathbf{h}\|^2}$. The random variables Z, C and G are one-to-one related to each other. We will use z, c and g for the realizations of Z, C and G respectively. Unlike f_e, the variables z, c and g are invariant to the locations of Eves but dependent on the small scale fading parameters $\mathbf{h}$ and g_B. For given realization of $\mathbf{h}$ and g_B, z is given. For $m = 0$, $Z = P_T\|\mathbf{h}\|^2$ has obviously a Chi-squared distribution with $2M$ DoF. For $m > 0$, one can prove the following lemma:

Lemma 2: If $m > 0$, the legitimate channel's SNR_{AB} (which is Z) has the following PDF (shown in Appendix C)

$$f_Z(z) = \frac{M\rho m(z\rho m)^{M-1}}{(1+z\rho m)^{M+1}}e^{\frac{1}{\rho P_J}}.\tag{23}$$

Proposition 2: Conditioned on $\mathbf{h}$ and g_B, the probability of achieving a secrecy rate strictly larger than R_s using the TAB scheme is given by

$$P_{con,\mathbf{h},g_B} = P_{con,z} = \exp\left[-\rho_E\int_0^R r\int_0^{2\pi}\Omega(\frac{1}{g};r,\theta)\mathrm{d}\theta\mathrm{d}r\right],\tag{24}$$

and hence $P_{con} = \int_0^{\infty}P_{con,z}f_Z(z)dz$ where

$$\Omega(\frac{1}{g};r,\theta) = \frac{e^{\frac{d_{BE}^{\alpha}}{P_J}}}{(1+\frac{f_e}{g})(1+\frac{\epsilon}{(M-1)g})^{M-1}}\tag{25}$$

and all other variables are defined before.

The proof is shown in Appendix D.

Remark 2: From (24) and (25), one can also verify the following subject to $P_T > 0$:

- For $\epsilon > 0$, $P_{con,\mathbf{h},g_B} \to 1$ as $P_T \to \infty$. $(1+\frac{\epsilon}{(M-1)g})^{M-1}$ converges to $e^{\epsilon/g}$ as M increases. For large P_T, $\frac{1-\frac{1}{\beta}}{(1-\epsilon)P_T} \approx 0$ so, $\frac{f_e}{g} = \left(\frac{d_{AEe}}{d_{BEe}}\right)^{\alpha}\frac{\|\mathbf{h}\|^2}{\beta(\frac{1}{P_J}+\rho|g_B|^2)}$ which is invariant to P_T and $\frac{\epsilon}{g} = \frac{\epsilon P_T\|\mathbf{h}\|^2}{\beta(1+\rho P_J|g_B|^2)}$ which goes to ∞ as $P_T\to\infty$.
- $P_{con,\mathbf{h},g_B}$ increases as ρ decreases. As ρ decreases, Z and c increase, and hence g and $\Omega(\frac{1}{g};r,\theta)$ decrease, and hence $P_{con,\mathbf{h},g_B}$ increases.
- If $\rho\to 0$, then $P_{con,\mathbf{h},g_B}\to 1$ as $P_J\to\infty$.
- If $\epsilon = 0$, the optimal P_J is ∞. If $\epsilon = 0$ then it follows from (24) and (25) that

$$P_{con,\mathbf{h},g_B} = \exp\left[-\rho_E\int_0^R r\int_0^{2\pi}\frac{e^{\frac{d_{BEe}^{\alpha}}{P_J}}}{1+\frac{f_e}{g}}\mathrm{d}\theta\mathrm{d}r\right],\tag{26}$$

  which is independent of P_T and monotonically increases as P_J increases. Thus the optimum P_J is ∞.
- For $\epsilon > 0$ and $P_T > 0$, the optimal P_J is a finite positive number. For $\epsilon > 0$ and $P_T > 0$, $\frac{f_e}{g}$ monotonically increases to $\frac{\|\mathbf{h}\|^2}{\beta\rho|g_B|^2}$ as $P_J\to\infty$ and $1+\frac{d_{BEe}^{\alpha}}{P_J}$ monotonically decreases to 1 as $P_J\to\infty$. So, $\frac{1+\frac{d_{BEe}^{\alpha}}{P_J}}{1+\frac{f_e}{g}}$ monotonically decreases to $\frac{1}{(1+\frac{\|\mathbf{h}\|^2}{\beta\rho|g_B|^2})}$ for $P_J\to\infty$. We can also observe that $\frac{\epsilon}{g}$ monotonically decreases to 0 for $P_J\to\infty$, so $\frac{1}{(1+\frac{\epsilon}{(M-1)g})^{M-1}}$ monotonically increases to 1 as $P_J\to\infty$. So, we can conclude that there is a finite positive P_J at which $P_{con,\mathbf{h},g_B}$ is maximized.

TABLE IV
EFFECTS OF PARAMETERS ON $\Omega(z,r,\theta)$ & $P_{con,z}$ WHEN $R_s = 0$

	$P_T \to \infty$	$P_J \to \infty$	$P_J \uparrow (\leq P_J^*)$	$P_J \uparrow (\geq P_J^*)$
$\Omega(z,r,\theta)\|_{\epsilon=0}$	$-$	$\downarrow \to const.$	$\downarrow$	$-$
$P_{con,z}, \epsilon = 0$	$-$	$\uparrow \to const.$	$\uparrow$	$-$
$\Omega(z,r,\theta)\|_{\epsilon\neq 0}$	$\to 0$	$\uparrow \to const.$	$\downarrow$	$\uparrow$
$P_{con,z}, \epsilon \neq 0$	$\to 1$	$\downarrow \to const.$	$\uparrow$	$\downarrow$

- For $R_s = 0$, $\Omega(\frac{1}{g}; r, \theta)$ is a decreasing function of ϵ which makes the upper bound of ϵ optimal. Furthermore, $\Omega(\frac{1}{g}; r, \theta)$ is rather flat around the optimal P_J, which makes it easy to find a practically optimal P_J.

The aforementioned observations are summarized in Table IV.

As shown in Appendix E, $\Omega(\frac{1}{g}; r, \theta)$ for any r and θ is a unimodal function with its minimum at a finite positive value of P_J. Therefore, $\int_0^R r \int_0^{2\pi} \Omega(\frac{1}{g}; r, \theta)\mathrm{d}\theta\mathrm{d}r$ must also have its minimum at a finite positive value of P_J, or equivalently $P_{con,z} = \exp(-\rho_E \int_0^R r \int_0^{2\pi} \Omega(\frac{1}{g}; r, \theta)\mathrm{d}\theta\mathrm{d}r)$ has its peak at that value of P_J.

Next, we consider two special cases for which the double integral in (24) can be simplified.

1) Bob in Full Duplex Mode With $\beta = 1$ and $\alpha = 2$: For $\beta = 1$ and $\alpha = 2$, it is shown in Appendix F that

$$\int_0^R \int_0^{2\pi} \Omega(z; r, \theta)\mathrm{d}\theta r\mathrm{d}r = \frac{2\pi}{(1+\frac{z\epsilon}{M-1})^{M-1}} \times \int_0^R \left(1 - \frac{1}{\sqrt{1+\frac{(r+d)^2}{r^2 zm}}\sqrt{1+\frac{(r-d)^2}{r^2 zm}}}\right) r\mathrm{d}r. \quad (27)$$

And $P_{out} = 1 - P_{con}$ versus P_J and ϵ will be illustrated in Fig. 4 from which we will see that for a given ϵ there is an optimal P_J and the optimal P_J is not very sensitive to ϵ.

Furthermore, if $P_J \to \infty$, then $z \to 0$, $zm \to \frac{\|\mathbf{h}\|^2}{\rho|g_B|^2}$ and (27) yields

$$\int_0^R \int_0^{2\pi} \Omega(z; r, \theta) d\theta r dr = 2\pi \int_0^R \left(1 - \frac{1}{\sqrt{1+\rho\frac{|g_B|^2}{\|\mathbf{h}\|^2}(1+\frac{d}{r})^2}\sqrt{1+\rho\frac{|g_B|^2}{\|\mathbf{h}\|^2}(1-\frac{d}{r})^2}}\right) r\mathrm{d}r. \quad (28)$$

Comparing (22) and (28), we see a similar structure of the two expressions. Since $\|\mathbf{h}\|^2 \geq \max_{i\in M} |h_i|^2$, the TAB scheme always yields a lower SOP than the TAS scheme.

Also note that if $\epsilon > 0$ and $P_T \to \infty$, then (27) implies that the SOP of the TAB scheme becomes one (similar to the case for TAS).

2) Bob in Half-Duplex Mode: In this case, we have $P_J = 0$ and $z = P_T\|\mathbf{h}\|^2$. Also assuming a large P_T, it is shown in Appendix G that

$$\int_0^R \int_0^{2\pi} \Omega(z; r, \theta)\mathrm{d}\theta r\mathrm{d}r = \frac{2\pi\beta^{\frac{2}{\alpha}}}{\alpha(\|\mathbf{h}\|^2)^{\frac{2}{\alpha}}(1+\frac{\epsilon P_T}{M-1}\frac{\|\mathbf{h}\|^2}{\beta})^{M-1}} \gamma\left(\frac{2}{\alpha}, \frac{R^\alpha\|\mathbf{h}\|^2}{\beta}\right). \quad (29)$$

Here $\gamma(\frac{2}{\alpha}, \frac{R^\alpha\|\mathbf{h}\|^2}{\beta})$ is the lower incomplete gamma function and increases monotonically as R increases. (29) is similar to (20) and is independent of P_T when $\epsilon = 0$. Since $\|\mathbf{h}\|^2 \geq \max_{i\in M} |h_i|^2$, the HD-TAB (even without using AN) results in a better secrecy performance than the HD-TAS. Note that the secrecy performance of the HD-TAB depends on P_T when $\epsilon > 0$. Furthermore, the term $\int_0^R \int_0^{2\pi} \Omega(z; r, \theta)\mathrm{d}\theta r\mathrm{d}r$ is inversely proportional to the factor $\left(1 + \frac{\epsilon P_T\|\mathbf{h}\|^2}{(M-1)g}\right)^{M-1}$. Thus, the term $\int_0^R \int_0^{2\pi} \Omega(z; r, \theta)\mathrm{d}\theta r\mathrm{d}r$ and hence SOP decreases as the number of transmit antenna M increases.

C. Secrecy Performance of the TAB-US Scheme

In [35], a TAS based downlink transmission scheme for multiple ordered half-duplex receivers or "a TAS based User Selection (US) scheme" was considered. In this section, we consider a TAB based counter part of the above scheme, which will be referred to as the TAB-US scheme.

As shown in Appendix H, we have

Proposition 3: For $\epsilon \geq 0$, the probability of achieving a secrecy rate strictly larger than R_s conditional on the distance of a selected user is

$$P[S_{AB} > R_s | d_{AB_n}] = \exp\left[\frac{-2\pi\rho_E}{\alpha} \frac{(\beta d_{AB_n}^\alpha)^M B(M-\frac{2}{\alpha}, \frac{2}{\alpha})}{(\frac{\epsilon P_T}{M-1})^{M-\frac{2}{\alpha}}} \times U(M-\frac{2}{\alpha}, 2-\frac{2}{\alpha}, \frac{(M-1)\beta d_{AB_n}^\alpha}{\epsilon P_T})\right] \quad (30)$$

where d_{AB_n} is the distance between Alice and the nth closest user, and U denotes the confluent hypergeometric function of the second kind [42].

With $P(S_{AB} > R_s | d_{AB_n})$ and $f_{d_{AB_n}}(x)$ from lemma 4 in Appendix I, one can readily compute the SOP $P(S_{AB} < R_s) = \int_0^\infty P(S_{AB} > R_s|x) f_{d_{AB_n}}(x)dx$ for any ϵ. We will show via simulation that the TAB-US scheme outperforms the TAS-US scheme.

As shown in Appendix I, for the special case of $\epsilon = 0$, $P(S_{AB} < R_s)$ can be simplified into:

$$P[S_{AB} > R_s] = \frac{1}{\left(1 + \frac{\rho_E}{\rho_U}\frac{2}{\alpha}\beta^{\frac{2}{\alpha}} B(M-\frac{2}{\alpha}, \frac{2}{\alpha})\right)^n}, \quad (31)$$

where $\frac{\rho_E}{\rho_U}$ is the ratio of the density of EDs over that of the legitimate receivers.

Furthermore, for $n = 1$ (the nearest Bob), (31) reduces to

$$P[S_{AB} < R_s] = 1 - \frac{1}{1 + \frac{\rho_E}{\rho_U}\frac{2}{\alpha}\beta^{\frac{2}{\alpha}} B(M-\frac{2}{\alpha}, \frac{2}{\alpha})}. \quad (32)$$

IV. SECRECY PERFORMANCE AGAINST COLLUDING EAVESDROPPERS

In this section, we consider the situation that EDs can share all information to decode the message. Since Alice knows the channel between Alice and Bob, the secrecy performance conditional on $\mathbf{h}$ and g_B is a useful measure. In one coherence period, $\mathbf{h}$ and g_B remains deterministic and study of closed form expression is important to find the optimal resource allocation strategy (i.e., how to choose ϵ and P_J). Considering $\mathbf{h}$ and g_B as deterministic makes the study completely different

from that in [33] as the Laplace trick used there can not be directly applied to derive the SOP closed form expression.

A. Full-Duplex Bob in the TAS Scheme

The SOP against colluding EDs conditional on $\mathbf{h}$ and g_B is

$$\begin{aligned} P[S_{AB}^{TAS} < R_s|\mathbf{h}, g_B] &= P\left[\frac{1+SNR_{AB}^{TAS}}{1+\sum\limits_{e\in\Phi} SNR_{AE_e}^{TAS}} < 2^{R_S}|\mathbf{h}, g_B\right] \\ &= P\left[\sum_{e\in\Phi}\frac{|h_{A_{i^*}E_e}|^2}{\frac{d_{AE_e}^{\alpha}}{P_T}+\frac{d_{AE_e}^{\alpha}}{d_{BE_e}^{\alpha}}mX_2} > y_0\right] \\ &= \int_{y_0}^{\infty} f_{I_e}(x)\mathrm{d}x \end{aligned} \tag{33}$$

where $I_e = \sum\limits_{e\in\Phi} SNR_{AE_e}^{TAS} = \sum\limits_{e\in\Phi}\frac{|h_{A_{i^*}E_e}|^2}{\frac{d_{AE_e}^{\alpha}}{P_T}+\frac{d_{AE_e}^{\alpha}}{d_{BE_e}^{\alpha}}mX_2}$ which is the sum of SNRs at all EDs. It is shown in Appendix J that the Laplace transform of the PDF of I_e is

$$\mathcal{L}_{I_e}(s) = \exp\left[-\rho_E\int_0^R\int_0^{2\pi}\frac{s}{f_e}\mathbf{E_1}(K(s))e^{K(s)}\mathrm{d}\theta r\mathrm{d}r\right] \tag{34}$$

where $\mathbf{E_1}(a) = \int_0^{\infty}\frac{e^{-ax}}{1+x}\mathrm{d}x$ is the so called exponential integral function of a and $K(s) = \frac{s+\frac{d_{AE_e}^{\alpha}}{P_T}}{f_e}$. Note that $\mathbf{E_1}(a)$ is monotonically decreasing function of a, and $K(s)$ is a strictly positive quantity. Later, we will discuss the relationship between $\mathbf{E_1}(K(s))$ and SOP.

We know that

$$\begin{aligned} P[S_{AB}^{TAS} < R_s|\mathbf{h}, g_B] &= P[\frac{I_e}{y_0} > 1] \\ &\lessapprox P[\frac{I_e}{y_0} > l] \\ &= \mathbb{E}\big[1-\exp(-\frac{aI_e}{y_0})\big]^N \\ &= \mathbb{E}\left[\sum_{n=0}^{N}\binom{N}{n}(-1)^n\exp(-\frac{an}{y_0}I_e)\right] \\ &= \sum_{n=0}^{N}\binom{N}{n}(-1)^n\mathcal{L}_{I_e}(\frac{an}{y_0}), \end{aligned} \tag{35}$$

where $\lessapprox$ denotes "less than and asymptotically equal to", and l is a normalized gamma distributed random variable with the shape parameter N, and as $N\to\infty$, l approaches its upper bound equal to 1 [39]–[41]. (Note that the left side of $\lessapprox$ is less than the right side if N is finite, or equals to the right side if $N\to\infty$.) Also $a = \frac{N}{(N!)^{\frac{1}{N}}}$, and y_0 is a realization of Y.

From (34) and (35), we have

Proposition 4: For the TAS scheme,

$$\begin{aligned} &P[S_{AB}^{TAS} < R_s|\mathbf{h}, g_B] \\ &\lessapprox\sum_{n=0}^{N}\binom{N}{n}(-1)^n\exp\left[-\rho_E\int_0^R\int_0^{2\pi}\frac{s}{f_e}\mathbf{E_1}(K(s))\right. \\ &\left.e^{K(s)}\mathrm{d}\theta r\mathrm{d}r\right]\Big|_{s=\frac{an}{y_0}} \end{aligned} \tag{36}$$

TABLE V

COMPARISON BETWEEN $\Psi(Y,r,\theta)$ AND $\Xi(s,r,\theta)|_{s=\frac{an}{y_0}}$ SUBJECT TO $R_s = 0$. THE COLUMN FOR $P_J\to\infty$ IS SUBJECT TO A FIXED ρP_J

	P_T	$P_J\to\infty$	$P_J\uparrow(\le {P_J}^*)$	$P_J\uparrow(\ge {P_J}^*)$
$\Psi(Y,r,\theta)$	$-$	$\to 0$	$\downarrow$	$\uparrow$
$\Xi(s,r,\theta)\|_{s=\frac{an}{y_0}}$	$-$	$\to const.$	$\downarrow$	$\uparrow$

where $s = \frac{an}{y_0}$, $K(s) = K(s)\big|_{s=\frac{an}{y_0}} = K(s)\big|_{s=\frac{an}{\frac{y}{\beta}-1+\frac{1}{\beta}}} = \frac{d_{BE_e}^{\alpha}}{P_J}+\frac{s}{f_e} = \frac{d_{BE_e}^{\alpha}}{P_J}+\frac{an}{f_e y_0}$. If $\beta=1$, we have $y_0 = y$ and then $K(s) = \frac{d_{BE_e}^{\alpha}}{P_J}+an\frac{d_{BE_e}^{\alpha}}{d_{AE_e}^{\alpha}}\frac{\frac{1}{P_J}+\rho|g_B|^2}{\max\limits_{i\in M}|h_i|^2}$ which is independent of P_T.

Remark 3: The secrecy performance is dependent on P_J throughout the term $\Xi(s,r,\theta)|_{s=\frac{an}{y_0}} = \frac{s}{f_e}\mathbf{E_1}(K(s))e^{K(s)}|_{s=\frac{an}{y_0}}$. One can verify that as P_J increases,

- $\frac{s}{f_e}e^{K(s)}$ decreases monotonically and saturates to a lower bound.
- $\mathbf{E_1}(K(s))$ increases monotonically and saturates to an upper bound.

These statements indicate that finding the optimal P_J to minimize $\Xi(s,r,\theta)|_{s=\frac{an}{y_0}}$ is similar to that of $\Psi(Y,r,\theta)$ for the non-colluding TAS scheme. A comparison between $\Psi(Y,r,\theta)$ and $\Xi(s,r,\theta)|_{s=\frac{an}{y_0}}$ is shown in Table V. Note that, optimum jamming power ${P_J}^*$ is not necessarily the same for $\Psi(Y,r,\theta)$ and $\Xi(s,r,\theta)|_{s=\frac{an}{y_0}}$. Finally, simulation result shows that as P_J increases, the conditional SOP in (36) achieves its minimum at a finite nonzero P_J.

B. Half-Duplex Bob in TAS Scheme

If Bob is in the HD mode, then the sum of ED's SNR is $I_e^{HD} = \sum\limits_{e\in\Phi}\frac{X'_{1,e}P_T}{d_{AE_e}^{\alpha}}$, where $X'_{1,e}$ is exponentially distributed with unit mean. One can verify that the Laplace transform of the PDF of I_e^{HD} is

$$\begin{aligned} \mathcal{L}_{I_e^{HD}}(s) &= E_{\Phi}\left[\prod_{e\in\Phi}\frac{1}{1+\frac{sP_T}{d_{AE_e}^{\alpha}}}\right] \\ &= \exp\left[-\rho_E\pi R^2\mathbf{F}(1,\frac{2}{\alpha};1+\frac{2}{\alpha};-\frac{R^{\alpha}}{sP_T})\right] \end{aligned} \tag{37}$$

where $\mathbf{F}(1,\frac{2}{\alpha};1+\frac{2}{\alpha};-\frac{R^{\alpha}}{sP_T})$ is known as the Gaussian hypergeometric function. Note that α is governed by the environment. So, only the last parameter $\frac{R^{\alpha}}{sP_T}$ in $\mathbf{F}(1,\frac{2}{\alpha};1+\frac{2}{\alpha};-\frac{R^{\alpha}}{sP_T})$ is controllable via P_T, which takes real value between 0 to ∞. One can verify that $\frac{R^{\alpha}}{sP_T}$ is independent of P_T for $\beta=1$, which is similar as non-colluding HD TAS scheme.

Replacing $\mathcal{L}_{I_e}$ in (35) by $\mathcal{L}_{I_e^{HD}}$ in (37) yields

$$\begin{aligned} P[S_{AB}^{TAS} < R_s|\mathbf{h}, g_B] \lessapprox \sum_{n=0}^{N}\binom{N}{n}(-1)^n\exp\Big[-\rho_E\pi R^2 \\ \mathbf{F}(1,\frac{2}{\alpha};1+\frac{2}{\alpha};-\frac{R^{\alpha}}{sP_T})\Big]\Big|_{s=\frac{an}{y_0}} \end{aligned} \tag{38}$$

where $s = \frac{an}{y_0}$. The result in (38) is that in (36) with $P_J = 0$ but the former is a much simplified form than the latter.

C. Full-Duplex Bob in TAB Scheme Without an From Alice

Conditional on $\mathbf{h}$ and g_B, the legitimate channel's SNR is z as previously defined. For $\epsilon = 0$ (i.e., without AN from Alice), the SNR at the eth Eve is (from (11)):

$$SNR_{AE_e}^{TAB} = \frac{X_1\Theta}{\frac{d_{AE_e}^{\alpha}}{P_T} + m\frac{d_{AE_e}^{\alpha}}{d_{BE_e}^{\alpha}}X_2} = \frac{X_4}{\frac{d_{AE_e}^{\alpha}}{P_T} + m\frac{d_{AE_e}^{\alpha}}{d_{BE_e}^{\alpha}}X_2}. \quad (39)$$

Similar to the analysis leading to (36), the SOP now is still given by (36) but with $s = \frac{an}{\frac{z}{\beta}-1+\frac{1}{\beta}}$. Hence, we have:

Proposition 5: For the TAB scheme with $\epsilon = 0$,

$$P[S_{AB}^{TAB} < R_s|\mathbf{h}, g_B] \lessapprox \sum_{n=0}^{N}\binom{N}{n}(-1)^n \exp\Big[-\rho_E\int_0^R\int_0^{2\pi}\frac{s}{f_e}\mathbf{E_1}(K(s)) e^{K(s)}\mathrm{d}\theta r\mathrm{d}r\Big]\Big|_{s=\frac{an}{\frac{z}{\beta}-1+\frac{1}{\beta}}}. \quad (40)$$

Since $\|\mathbf{h}\|^2 \geq \max_{i\in M}|h_i|^2$, the TAB scheme always outperforms the TAS scheme.

1) Bob in Half-Duplex Mode: In this case, we have $P_J = 0$ and $z = P_T\|\mathbf{h}\|^2$. The SOP expression is similar to (38) and can be expressed as

$$P[S_{AB}^{TAB} < R_s|\mathbf{h}, g_B] \lessapprox \sum_{n=0}^{N}\binom{N}{n}(-1)^n \exp\Big[-\rho_E\pi R^2 \mathbf{F}(1,\frac{2}{\alpha};1+\frac{2}{\alpha};-\frac{R^{\alpha}}{sP_T})\Big]\Big|_{s=\frac{an}{\frac{z}{\beta}-1+\frac{1}{\beta}}}. \quad (41)$$

D. Full-Duplex Bob in TAB Scheme With an From Alice

For the TAB scheme with $\epsilon > 0$, we have

$$P[S_{AB}^{TAB} < R_s|\mathbf{h}, g_B] = P[\frac{1+SNR_{AB}^{TAB}}{1+\sum_{e\in\Phi}SNR_{AE_e}^{TAB}} < 2^{R_S}|\mathbf{h}, g_B]$$

$$\overset{(a)}{\lessapprox} P[\sum_{e\in\Phi}\frac{X_4}{\frac{\epsilon}{M-1}X_{4,4}+f_eX_2} > \frac{z}{\beta}+\frac{\frac{1}{\beta}-1}{1-\epsilon}]$$

$$\overset{(b)}{\lessapprox} \sum_{n=0}^{N}\binom{N}{n}(-1)^n\mathcal{L}_{\tilde{I}_e}\Big(\frac{an}{\frac{z}{\beta}+\frac{\frac{1}{\beta}-1}{1-\epsilon}}\Big) \quad (42)$$

where the parameters defined after (13) have been applied and $\tilde{I}_e = \sum_{e\in\Phi}\frac{X_4}{\frac{\epsilon}{M-1}X_{4,4}+f_eX_2}$. Here, (a) is due to neglecting the background noise $n_{A,E_e}(k)$ at Eve (but not the noise at Bob), and (b) is due to the application of the normalized gamma random variable as discussed before. Similar to that in Appendix J, one can verify

$$\mathcal{L}_{\tilde{I}_e}(s) = \exp\Big[-\rho_E s\int_0^R\int_0^{2\pi}\int_{x=0}^{\infty}\frac{e^{-sx}}{(1+f_ex)}\times\frac{1}{(1+\frac{\epsilon}{M-1}x)^{M-1}}\mathrm{d}x\mathrm{d}\theta r\mathrm{d}r\Big]. \quad (43)$$

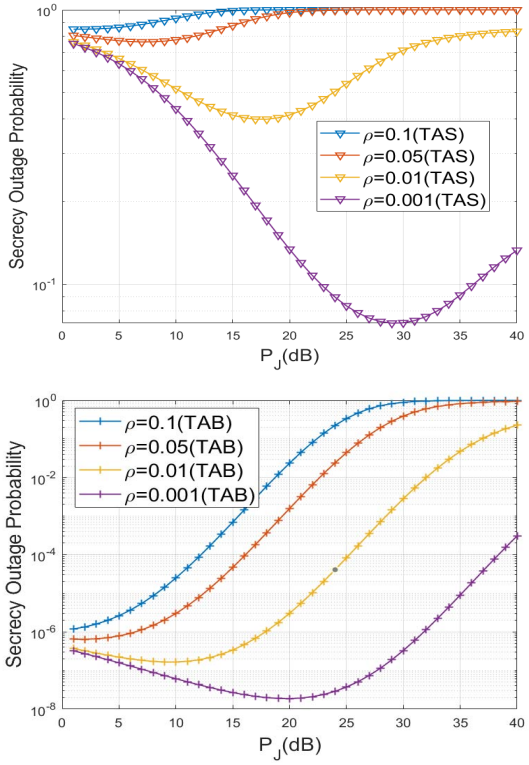

Fig. 2. Comparison of the TAS and TAB schemes in terms of P_{out} against non-colluding EDs.

V. Simulations

In this section, we illustrate the secrecy outage probabilities (SOP) of the TAS and TAB schemes against randomly located EDs. We consider both colluding and non-colluding cases. Most of our simulation results provide comparisons between TAS and TAB schemes. Moreover, we present the secrecy performance enhancement of the TAB scheme using AN.

Throughout the simulations, we will assume unit noise variance, $\alpha = 2$, $P_T = 40$ dB, $R_D = 4$ b/s/Hz, $\rho_E = 1$, $M = 5$, $d = 1$ and $R = 5$. Unless otherwise specified, we let P_J, ρ and ϵ be 40 dB, 0.01 and 0.01 respectively. Since Alice can estimate the legitimate channel and know the self interference channel of Bob, therefore, we will first study the SOP under conditional $\mathbf{h}$ and g_B for the TAB scheme. Considering $R_D = 4$, ϵ can be set between 0 and 0.53 to maintain a nonzero desired data transmission for the above given ρ and P_J.

In Fig. 2, the SOP of the TAS and TAB schemes for non-colluding EDs is illustrated under different values of P_J and ρ. For the TAB scheme, $\epsilon = 0$ is chosen. We see that as ρ decreases, the optimum jamming power increases which results in lower SOP for both TAS and TAB

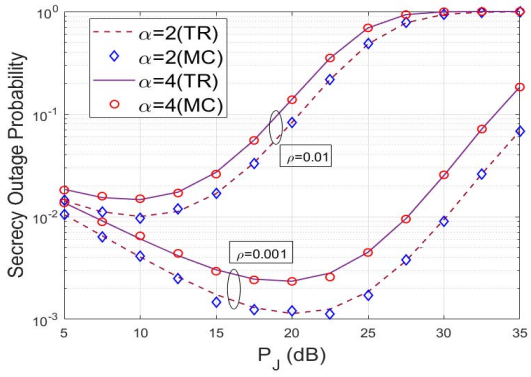

Fig. 3. Comparison of theoretical results ("TR") and simulation results ("MC") of the TAB scheme in terms of P_{out} versus P_J.

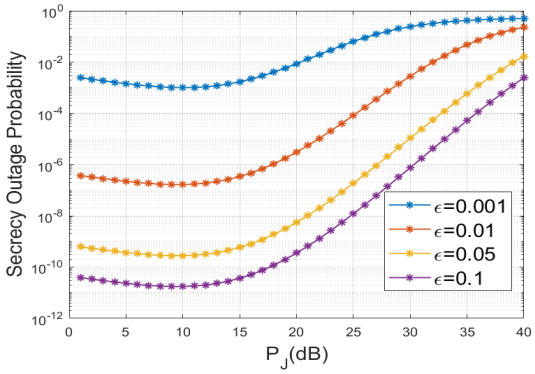

Fig. 4. Illustration of $P_{out} = 1 - P_{con}$ versus P_J and ϵ for the TAB scheme.

schemes. And the TAB scheme outperforms the TAS scheme substantially.

In Fig. 3, we compare the Monte Carlo (MC) simulation results (using $N_R = 10^5$ independent runs) with our theoretical results shown in (24) where $R = 5$ and $\rho_E = 10$. We observe that the two results match each other very well. This consistency between theory and simulation holds for all other results we have tested under a sufficiently large N_R.

Fig. 4 shows the SOP of the TAB scheme with $\epsilon > 0$. We see that the SOP decreases as ϵ increases, the optimal value of P_J is dependent on ϵ but the dependence is rather weak (or not very sensitive).

To illustrate the TAS and TAB schemes with user selection (i.e., TAS-US and TAB-US), we consider $P_T = 50$ dB, $\alpha = 2$, $\beta = 2$, $\epsilon = 0.00001$, $\rho_U = 0.5$ and $\rho_E = 0.1$ unless otherwise specified.

Fig. 5 shows the SOP of the TAS-US and TAB schemes for the nearest user. As the number M of transmit antennas increases, the performance gap between TAB-US and TAS-US increases rapidly for $\epsilon > 0$. More importantly, we see that only a small fraction (e.g., $\epsilon = 0.00001$ or $\epsilon P_T = 0$ dB which is at the same level as the noise variance) of the transmit power used for AN makes a huge difference.

Fig. 6 illustrates the effects of ED's density ρ_E on the SOP of TAS-US and TAB-US for the nearest user. And Fig. 7 illustrates the effects of the users' density ρ_U on the SOP of TAS-US and TAB-US for the nearest user. We see that SOP increases as ρ_E increases but decreases as ρ_U increases. The performance gap between TAS-US and TAB-US remains

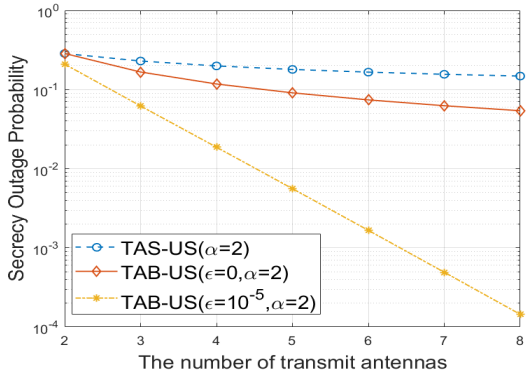

Fig. 5. SOP of TAS-US and TAB-US for the nearest user vs the number of transmit antennas against non-colluding EDs.

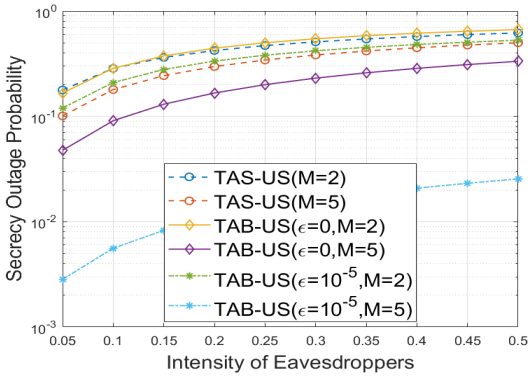

Fig. 6. SOP vs intensity of eavesdroppers for ordered users against non-colluding EDs.

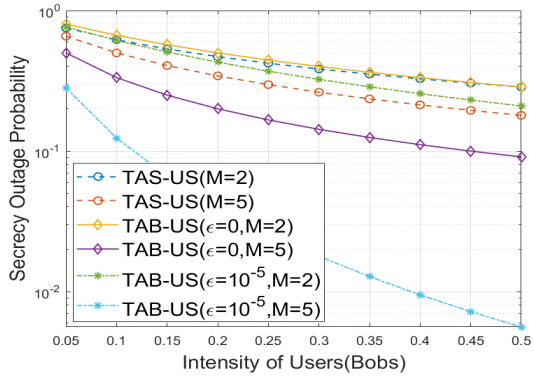

Fig. 7. SOP vs intensity of users against non-colluding EDs.

approximately the same as ρ_E increases but increases as ρ_U increases.

Fig. 8 shows the SOP of the TAS-US and TAB-US schemes as functions of the order index (n) of users (from nearest to farthest). We see that the SOP increases as n increases and the performance gap between TAB-US and TAS-US reduces as n increases.

Now, we consider the TAB and TAS schemes for colluding EDs. We assume that there are two circles of radii R_g and R around Alice, and EDs exist and collude within the two circles. In our experiment, we let $R_g = 0.1$ and $R = 5$. Although the closed form expressions of the SOP in this case are all in series expansions, choosing $N = 20$ (e.g., see (36)) provided good approximations.

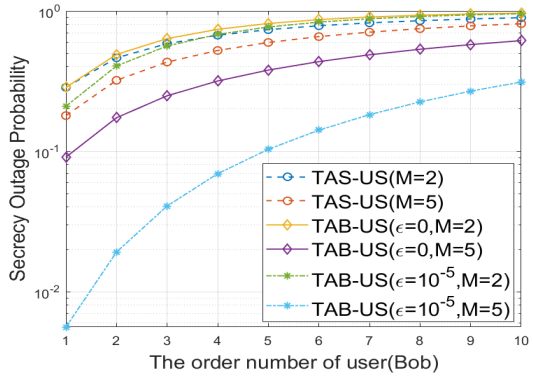

Fig. 8. SOP vs the order number of user against non-colluding EDs.

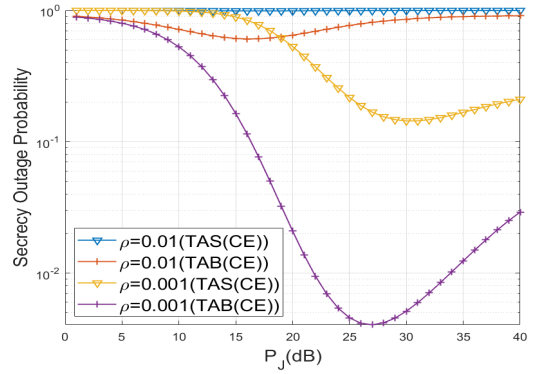

Fig. 9. Comparison of the TAB and TAS schemes in terms of P_{out} against colluding EDs.

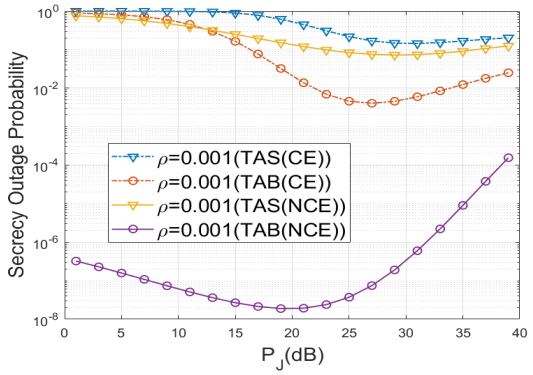

Fig. 10. Comparison of the TAB and TAS schemes in terms of P_{out} against colluding and non-colluding EDs.

Fig. 9 shows the SOP of TAS and TAB schemes for colluding EDs as functions of the self-interference power gain ρ and the jamming power P_J from full-duplex Bob. We see that the optimal P_J increases as the self-interference power gain ρ decreases, and the optimized SOP reduces significantly as ρ decreases.

Finally, Fig. 10 illustrates the differences of SOP for colluding and non-colluding EDs. We see that the performance gap between colluding and non-colluding is large. But the TAB scheme is consistently better than the TAS scheme in terms of SOP.

VI. Conclusion

In this paper, we presented closed form expressions of secrecy outage probabilities (SOP) of several schemes for multi-antenna downlink transmissions against randomly located eavesdroppers (EDs). We considered both transmit antenna selection (TAS) and transmit antenna beamforming (TAB) schemes, full-duplex (FD) and half-duplex (HD) receivers/users, colluding and non-colluding EDs, the use of artificial noise (AN) from transmitter, and user selection based on their distances to the transmitter. For all these schemes and scenarios, we assume that EDs are distributed as the Poisson Point Process (PPP). For user selection, we also assume the PPP model for users' locations. The closed-form expressions of SOP are useful for numerical computations needed for network design purposes. We provided numerical examples to illustrate the usefulness of these expressions, which also revealed important observations such as the optimal jamming power from FD users and the impacts of several other parameters on SOP.

Appendix A
Proof of (14)

It follows from (1), (7) and (8) that

$$\begin{aligned} P_{con,\Phi,Y} &\triangleq P[S_{AB}^{TAS} > R_s|\Phi, Y] \\ &= P\left[\frac{1+SNR_{AB}^{TAS}}{1+\max\limits_{e\in\Phi} SNR_{AE_e}^{TAS}} > 2^{R_S}\middle|\Phi, Y\right] \\ &= P\left[\max_{e\in\Phi} SNR_{AE_e}^{TAS} < Y_0\middle|\Phi, Y\right] \\ &= \prod_{e\in\Phi} P\left[\frac{|h_{A_{i^*}E_e}|^2}{\frac{d_{AE_e}^{\alpha}}{P_T}+\frac{d_{AE_e}^{\alpha}}{d_{BE_e}^{\alpha}}m|h_{BE_e}|^2} < Y_0\middle|\Phi, Y\right] \\ &= \prod_{e\in\Phi}\big(1-\Psi(Y, r_e, \theta_e)\big), \end{aligned} \tag{44}$$

where (due to the lemma shown next)

$$\Psi(Y, r_e, \theta_e) = \frac{\exp(-\frac{d_{AE_e}^{\alpha}}{P_T}Y_0)}{1+m(\frac{d_{AE_e}}{d_{BE_e}})^{\alpha}Y_0}$$

We have applied the following lemma.

Lemma 3: If A and B (like $|h_{A_{i^*}E_e}|^2$ and $|h_{BE_e}|^2$) are two independent random variables with the exponential distribution of unit mean, then $P(\frac{A}{a+bB} < c) = 1-\frac{e^{-ac}}{1+bc}$.

Note that we are only interested in such R_s that $\log_2(1+SNR_{AB}) \geq R_s$, which implies $Y_0 \geq 0$.

Let $P_{con,Y}$ be P_{con} conditional only on Y. Applying the Campbell's theorem [38] to (44) yields:

$$\begin{aligned} P_{con,Y} &= \mathbb{E}_{\Phi}\{P[SNR_{AB}^{TAS} > R_s|\Phi, Y]\} \\ &= \exp\left[-\rho_E\int_0^R\int_0^{2\pi}\Psi(Y, r, \theta)r\,\mathrm{d}\theta\mathrm{d}r\right]. \end{aligned}$$

Appendix B
A Simplification of the Double Integral in (14)

Assume $R_s = 0$ and $\alpha = 2$. Then, $\beta = 1$ and $Y_0 = Y$. Let the distance between Alice and Bob be d. Then, $\frac{d_{AE}^{\alpha}}{d_{BE}^{\alpha}} = \frac{d_{AE}^2}{d_{BE}^2} = \frac{r^2}{r^2+d^2-2rd\cos\theta}$, and

furthermore

$$\begin{aligned}
&\int_0^R \int_0^{2\pi} \Psi(Y,r,\theta) r \mathrm{d}\theta \mathrm{d}r \\
&= \int_0^R \int_0^{2\pi} \frac{\exp(-\frac{Yr^2}{P_T})}{1+mY\frac{r^2}{r^2+d^2-2rd\cos\theta}} r\mathrm{d}\theta\mathrm{d}r \\
&= \int_0^R \int_0^{2\pi} \exp(-\frac{Yr^2}{P_T}) \\
&\quad \times \frac{\big((1+mY)r^2+d^2-2rd\cos\theta\big)-mYr^2}{(1+mY)r^2+d^2-2rd\cos\theta} r\mathrm{d}\theta\mathrm{d}r \\
&= 2\pi \int_0^R \exp(-\frac{Yr^2}{P_T}) r\mathrm{d}r \\
&\quad - \int_0^R \int_0^{2\pi} \frac{mYr^3\exp(-\frac{Yr^2}{P_T})}{(1+mY)r^2+d^2-2rd\cos\theta}\mathrm{d}\theta\mathrm{d}r, \quad (45)
\end{aligned}$$

where the first term can be obviously reduced. The second term in (45), can be simplified by applying $\int_0^{2\pi} \frac{1}{a-b\cos\theta}\mathrm{d}\theta = \frac{2\pi}{\sqrt{a^2-b^2}}$ identity. Then, (45) yields

$$\begin{aligned}
&\int_0^R \int_0^{2\pi} \Psi(Y,r,\theta) r \mathrm{d}\theta \mathrm{d}r \\
&= \frac{\pi P_T}{Y}\left(1-\exp\left(-\frac{YR^2}{P_T}\right)\right) - 2\pi mY \\
&\quad \times \int_0^R \frac{r^3\exp(-\frac{Yr^2}{P_T})}{\sqrt{\big((1+mY)r^2+d^2\big)^2-4r^2d^2}}\mathrm{d}r \\
&= \frac{\pi P_T}{Y}\left(1-\exp\left(-\frac{YR^2}{P_T}\right)\right) - \pi mY \\
&\quad \times \int_0^{R^2} \frac{\exp\left(-\frac{Yr}{P_T}\right) r}{\sqrt{\big((1+mY)r+d^2\big)^2-4rd^2}}\mathrm{d}r. \quad (46)
\end{aligned}$$

which is a much simplified expression of the double integral in (14).

Appendix C
Proof of Lemma 2

Here, $Z = \frac{\|\mathbf{h}\|^2}{\frac{1}{P_T}+\rho m|g_B|^2}$. Lets consider, $Y_3 = \|\mathbf{h}\|^2$, $Y_2 = \frac{1}{P_T}+\rho m|g_B|^2$ and $Z = \frac{Y_3}{Y_2}$. Note that $f_{Y_3}(x) = \frac{1}{\Gamma(M)}x^{M-1}e^{-x}$ and $f_{Y_2}(x) = \frac{1}{\rho m}exp(-\frac{x-\frac{1}{P_T}}{\rho m}), x > \frac{1}{P_T}$.

$$\begin{aligned}
F_Z(z) &= P[\frac{Y_3}{Y_1} < z] \\
&= P[|g_B|^2 > \frac{Y_3 - \frac{z}{P_T}}{z\rho m}] \\
&= \int_{y=0}^{\infty} f_{Y_3}(y)dy \int_{x=\frac{y-\frac{z}{P_T}}{z\rho m}}^{\infty} e^{-x}dx \\
&= \frac{1}{\Gamma(M)}\int_{y=0}^{\infty} y^{M-1}e^{-y}e^{-\frac{y-\frac{z}{P_T}}{z\rho m}}dy \\
&= \frac{e^{\frac{1}{\rho P_J}}}{\Gamma(M)(1+\frac{1}{z\rho m})^M}\int_{y=0}^{\infty}\big(y(1+\frac{1}{z\rho m})\big)^{M-1} \\
&\quad \times e^{-y(1+\frac{1}{z\rho m})}d\big(y(1+\frac{1}{z\rho m})\big) \\
&= \frac{e^{\frac{1}{\rho P_J}}}{(1+\frac{1}{z\rho m})^M}. \quad (47)
\end{aligned}$$

If $m > 0$ then, $f_Z(z) = e^{\frac{1}{\rho P_J}} M\rho m \frac{z\rho m^{M-1}}{(1+z\rho m)^{M+1}}$. Ror $m = 0$, Z follows scaled CHI squared distribution.

Appendix D
Proof of (24)

The secrecy of the TAB scheme can be analyzed as follows.

$$\begin{aligned}
P_{con,\Phi,\mathbf{h},g_B} &\triangleq P[S_{AB} > R_S|\Phi,\mathbf{h},g_B] \\
&= P[S_{AB} > R_S|\Phi,z] \\
&= P\left[\max_{e\in\Phi} SNR_{AE_e}^{TAB} < \frac{SNR_{AB}}{\beta} - (1-\frac{1}{\beta})\middle|\Phi,z\right] \\
&= P\Bigg[\max_{e\in\Phi} \frac{X_1\Theta}{d_{AE}^{\alpha} + \frac{P_J d_{AEe}^{\alpha}}{d_{BEe}^{\alpha}}X_2 + \frac{\epsilon P_T}{M-1}X_1(1-\Theta)} \\
&\quad < \frac{\|\mathbf{h}\|^2}{\beta(1+\rho|g_B|^2P_J)} - \frac{1-\frac{1}{\beta}}{(1-\epsilon)P_T}\Bigg|\Phi,z\Bigg] \\
&= \prod_{e\in\Phi} P\Bigg[\frac{X_1\Theta}{\frac{P_J d_{AEe}^{\alpha}}{d_{BEe}^{\alpha}}\left(X_2+\frac{d_{BE}^{\alpha}}{P_J}\right) + \frac{\epsilon P_T}{M-1}X_1(1-\Theta)} \\
&\quad < c\Big|\Phi,z\Bigg] \\
&= \prod_{e\in\Phi} P\left[\Theta < \frac{\frac{\epsilon}{M-1}+f_e\frac{X_3}{X_1}}{\frac{\epsilon}{M-1}+g}\middle|\Phi,z\right], \quad (48)
\end{aligned}$$

where $X_3 = X_2 + \frac{d_{BE}^{\alpha}}{P_J}$, and X_1, X_2 and $\boldsymbol{\Theta}$ are independent variables as defined previously (after (11)). It is easy to verify that $f_{\frac{X_2}{X_1}}(x) = M(1+x)^{-(M+1)}$, which is similar to the $F(2,2M)$ distribution [37]. When large scale channel gain of jamming signal at ED is higher than noise level, i.e., $\frac{P_J}{d_{BE}^{\alpha}} \gg 1$, the shift between X_3 and X_2 becomes smaller. Furthermore, one can verify that $f_{\frac{X_3}{X_1}}(x) \approx e^{\frac{d_{BE}^{\alpha}}{P_J}} M(1+x)^{-(M+1)}$. It follows from the PDF $f_{\Theta}(x)$ shown earlier that the CDF of Θ is $F_{\Theta}(x) = 1-(1-x)^{M-1}$. Then, it is shown in Appendix D-A that

$$P\left[\Theta > \frac{\frac{\epsilon}{M-1}+f_e\frac{X_3}{X_1}}{\frac{\epsilon}{M-1}+g}|\Phi,z\right] = \frac{e^{\frac{d_{BE}^{\alpha}}{P_J}}}{(1+\frac{f_e}{g})(1+\frac{\epsilon}{(M-1)g})^{M-1}}, \quad (49)$$

where g is a function of Z as defined before. Averaging over the PPP distribution of the locations of the Eves, one can verify (using the Campbell's theorem) that

$$\begin{aligned}
P_{con,\mathbf{h},g_B} &= P_{con,z} \triangleq \mathbb{E}_{\Phi}\{P[S_{AB} > R_S|\Phi,\mathbf{h},g_B]\} \\
&= \mathbb{E}_{\Phi}\left[\prod_{e\in\Phi}\left(1-P\left[\Theta > \frac{\frac{\epsilon}{M-1}+f_e\frac{X_3}{X_1}}{\frac{\epsilon}{M-1}+g}|\Phi,z\right]\right)\right]
\end{aligned}$$

$$= \mathbb{E}_\Phi\left[\prod_{e\in\Phi}\left(1-\frac{e^{\frac{d_{BE}^\alpha}{P_J}}}{(1+\frac{f_e}{g})(1+\frac{\epsilon}{(M-1)g})^{M-1}}\right)\right]$$
$$= \exp\left[-\rho_E\int_0^R r\int_0^{2\pi}\Omega(\frac{1}{g};r,\theta)\mathrm{d}\theta\mathrm{d}r\right],$$

where z is a realization of Z, g is a function of z, and

$$\Omega(\frac{1}{g};r,\theta)=\frac{e^{\frac{d_{BE}^\alpha}{P_J}}}{(1+\frac{f_e}{g})(1+\frac{\epsilon}{(M-1)g})^{M-1}}.$$

A. Proof of (49)

The complement of (49) is

$$P[\Theta<\frac{\frac{\epsilon}{M-1}+f_e\frac{X_3}{X_1}}{\frac{\epsilon}{M-1}+g}|\Phi,z]$$
$$=\int_0^\infty F_\Theta\left(\frac{\frac{\epsilon}{M-1}+f_ex}{\frac{\epsilon}{M-1}+g}\right)f_{\frac{X_3}{X_1}}(x)\mathrm{d}x$$
$$=\int_0^{\frac{g}{f_e}} F_\Theta\left(\frac{\frac{\epsilon}{M-1}+f_ex}{\frac{\epsilon}{M-1}+g}\right)f_{\frac{X_3}{X_1}}(x)\mathrm{d}x$$
$$+\int_{\frac{g}{f_e}}^\infty F_\Theta\left(\frac{\frac{\epsilon}{M-1}+f_ex}{\frac{\epsilon}{M-1}+g}\right)f_{\frac{X_3}{X_1}}(x)\mathrm{d}x. \quad (50)$$

Here, $F_\Theta(y)=1$ for $y\geq 1$, so $F_\Theta\left(\frac{\frac{\epsilon}{M-1}+f_ex}{\frac{\epsilon}{M-1}+g}\right)=1$ for $x\geq\frac{g}{f_e}$. Then (50) continues as follows:

$$\int_0^{\frac{g}{f_e}} F_\Theta\left(\frac{\frac{\epsilon}{M-1}+f_ex}{\frac{\epsilon}{M-1}+g}\right)f_{\frac{X_3}{X_1}}(x)\mathrm{d}x+\int_{\frac{g}{f_e}}^\infty f_{\frac{X_3}{X_1}}(x)\mathrm{d}x$$
$$=\int_0^{\frac{g}{f_e}}\left[1-\left(1-\frac{\frac{\epsilon}{M-1}+f_ex}{\frac{\epsilon}{M-1}+g}\right)^{M-1}\right]f_{\frac{X_3}{X_1}}(x)\mathrm{d}x$$
$$+1-\int_{x=0}^{\frac{g}{f_e}} f_{\frac{X_3}{X_1}}(x)\mathrm{d}x$$
$$=1-\frac{Me^{\frac{d_{BE_e}^\alpha}{P_J}}g^{M-1}}{(\frac{\epsilon}{M-1}+g)^{M-1}}\int_0^{\frac{g}{f_e}}\left(\frac{1-\frac{f_e}{g}x}{1+x}\right)^{M-1}\frac{\mathrm{d}x}{(1+x)^2}. \quad (51)$$

Let $k=\frac{f_e}{g}$ and $z=\frac{1}{1+x}$. Then $(\frac{1-kx}{1+x})^{M-1}=k^{M-1}\big(-1+z\frac{k+1}{k}\big)^{M-1}$. The above leads to

$$P[\Theta<\frac{\frac{\epsilon}{M-1}+f_e\frac{X_3}{X_1}}{\frac{\epsilon}{M-1}+g}|\Phi,z]$$
$$=1-\frac{Me^{\frac{d_{BE_e}^\alpha}{P_J}}(gk)^{M-1}}{(\frac{\epsilon}{M-1}+g)^{M-1}}\int_{\frac{k}{k+1}}^1\big(-1+z(\frac{k+1}{k})\big)^{M-1}\mathrm{d}z. \quad (52)$$

Now, using $y=z(\frac{k+1}{k})-1$, we have

$$P[\Theta<\frac{\frac{\epsilon}{M-1}+f_e\frac{X_3}{X_1}}{\frac{\epsilon}{M-1}+g}|\Phi,\mathbf{h},g_B]$$
$$=1-\frac{Me^{\frac{d_{BE_e}^\alpha}{P_J}}k^M}{(1+k)(1+\frac{\epsilon}{(M-1)g})^{M-1}}\int_{y=0}^{y=\frac{1}{k}}y^{M-1}\mathrm{d}y$$
$$=1-\frac{e^{\frac{d_{BE_e}^\alpha}{P_J}}}{(1+\frac{f_e}{g})(1+\frac{\epsilon}{(M-1)g})^{M-1}}. \quad (53)$$

APPENDIX E
UNIMODALITY OF Ω

From (25), we have

$$\Omega(\frac{1}{g};r,\theta)=\underbrace{\frac{e^{\frac{d_{BE_e}^\alpha}{P_J}}}{\left(1+\frac{f_e}{g}\right)}}_{\Omega_1(P_J)}\underbrace{\frac{1}{\left(1+\frac{\epsilon}{(M-1)g}\right)^{M-1}}}_{\Omega_2(P_J)}, \quad (54)$$

where $\Omega_1(P_J)$ and $\Omega_2(P_J)$ are shown below to be positive and strictly monotonically decreasing and increasing functions, respectively, w.r.t. P_J, i.e., $\Omega_1'(P_J)<0$ and $\Omega_2'(P_J)>0$ for any $P_J\geq 0$. We will apply $x=\frac{1}{P_J}$ where $x\in(0,\infty)$ as $P_J\in(0,\infty)$. Now, recall $f_e=(\frac{d_{AE_e}}{d_{BE_e}})^\alpha\frac{P_J}{P_T}$ and $g=\frac{\beta(1+\rho P_J|g_B|^2)}{P_T\|\mathbf{h}\|^2}$. Then, it follows that

$$\Omega_1(x)=e^{xd_{BE_e}^\alpha}\left(1-\frac{k_e}{x+k_e+\rho|g_B|^2}\right)$$
$$\Omega_1'(x)=\Omega_1(x)\left(d_{BE_e}^\alpha+\frac{k_e}{(x+k_e+\rho|g_B|^2)(x+\rho|g_B|^2)}\right), \quad (55)$$

where $k_e=\left(\frac{d_{AE_e}}{d_{BE_e}}\right)^\alpha\frac{\|\mathbf{h}\|^2}{\beta}$, and $\Omega_1(x)$ and $\Omega_1'(x)$ are strictly positive. Also,

$$\Omega_2(x)=\frac{1}{\left(1+\frac{kx}{x+\rho|g_B|^2}\right)^{M-1}}$$
$$\Omega_2'(x)=-\Omega_2(x)\frac{(M-1)k\rho|g_B|^2}{(x+kx+\rho|g_B|^2)(x+\rho|g_B|^2)}, \quad (56)$$

where $k=\frac{\epsilon P_T\|\mathbf{h}\|^2}{(M-1)\beta}$, and $\Omega_2(x)$ and $\Omega_2'(x)$ are strictly positive and negative respectively.

Next, we will show that $\Omega(x)=\Omega_1(x)\Omega_2(x)$ is a unimodal function with minimum at a finite nonzero x. Consider the following stationary condition on x $\Omega'(x)=\Omega_1(x)\Omega_2'(x)+\Omega_2(x)\Omega_1'(x)=0$ or equivalently $\frac{\Omega_2'(x)}{\Omega_2(x)}=-\frac{\Omega_1'(x)}{\Omega_1(x)}$ which can be further reduced to

$$\frac{\Omega_2'(x)}{\Omega_2(x)}=-\frac{\Omega_1'(x)}{\Omega_1(x)}$$
$$d_{BE_e}^\alpha+\frac{M}{x+\rho|g_B|^2}=\frac{1}{x+k_e+\rho|g_B|^2}+\frac{M-1}{x+\frac{\rho|g_B|^2}{k+1}}. \quad (57)$$

Using $y=x+\rho|g_B|^2$ in (57) and after some algebraic manipulations, we get

$$y^3+\left(k_e-\frac{k\rho|g_B|^2}{k+1}\right)y^2+\left(\frac{k_e}{d_{BE_e}^\alpha}-\frac{k\rho|g_B|^2}{k+1}(k_e+\frac{M-1}{d_{BE_e}^\alpha})\right)y-\frac{Mk_ek\rho|g_B|^2}{d_{BE_e}^\alpha(k+1)}=0, \quad (58)$$

which is a cubic polynomial equation. Based on the characteristics of cubic polynomials, (58) has one, two or three roots

and one inflection point [43]. Furthermore, a cubic function is anti-symmetric around its inflection point. To show that (58) has only one positive solution, we just need to show that the inflection point is negative. The inflection point is where the second-order derivative of the cubic function is zero, i.e., $6y - 2(k_e - \frac{k\rho|g_B|^2}{k+1}) = 0$, or equivalently $x = -\frac{2k+3}{3(k+1)}\rho|g_B|^2 - \frac{k_e}{3}$, which in this case is indeed negative.

Finally, it is easy to verify that $\Omega(\frac{1}{g}; r, \theta)$ is a decreasing function of P_J at $P_J = 0$. Therefore, we have shown that $\Omega(\frac{1}{g}; r, \theta)$ for any r and θ has its minimum at a positive finite P_J.

Appendix F
Proof of (27)

Assume $\alpha = 2$ and $\beta = 1$. Then, $g = 1/z$, and

$$\begin{aligned}
&\int_0^R \int_0^{2\pi} \Omega(z; r, \theta)\mathrm{d}\theta r\mathrm{d}r \\
&= \frac{1}{(1+\frac{z\epsilon}{M-1})^{M-1}} \int_0^R \int_0^{2\pi} \frac{1}{1+zm\frac{r^2}{r^2+d^2-2rdcos\theta}}\mathrm{d}\theta r\mathrm{d}r \\
&= \frac{1}{(1+\frac{z\epsilon}{M-1})^{M-1}} \int_0^R \int_0^{2\pi} \Big(1 \\
&\quad - \frac{zmr^2}{(1+zm)r^2+d^2-2rdcos\theta}\Big)\mathrm{d}\theta r\mathrm{d}r, \qquad (59)
\end{aligned}$$

where

$$\begin{aligned}
&\int_0^{2\pi} \Big(1 - \frac{zmr^2}{(1+zm)r^2+d^2-2rdcos\theta}\Big)\mathrm{d}\theta \\
&\qquad = 2\pi\left(1 - \frac{1}{\sqrt{1+\frac{(r+d)^2}{r^2zm}}\sqrt{1+\frac{(r-d)^2}{r^2zm}}}\right). \qquad (60)
\end{aligned}$$

Combining (59) and (60) yields (27).

Appendix G
Proof of (29)

Assuming $P_J = 0$ and a large P_T, it follows that $c = \frac{\|\mathbf{h}\|^2}{\beta} - \frac{1-\frac{1}{\beta}}{(1-\epsilon)P_T} \approx \frac{\|\mathbf{h}\|^2}{\beta}$ and $z = P_T\|\mathbf{h}\|^2$. And from (48), we have

$$\begin{aligned}
&P[S_{AB} > R_S|\Phi, \mathbf{h}, g_B] \\
&= \prod_{e\in\Phi} P\Big[\frac{X_1\Theta}{d_{AE_e}^\alpha + \frac{\epsilon P_T}{M-1}X_1(1-\Theta)} < c|\Phi, \mathbf{h}, g_B\Big] \\
&= \prod_{e\in\Phi} P\Big[\frac{X_4}{d_{AE_e}^\alpha + \frac{\epsilon P_T}{M-1}X_{4,4}} < \frac{\|\mathbf{h}\|^2}{\beta}|\Phi, \mathbf{h}, g_B\Big], \qquad (61)
\end{aligned}$$

where $X_4 = \Theta X_1$ is exponentially distributed with mean $= 1$ and $X_{4,4} = (1-\Theta)X_1$ is independent of X_4 and has the $\Gamma(M-1, 1)$ distribution. Then,

$$\begin{aligned}
&P\Big[\frac{X_4}{d_{AE_e}^\alpha + \frac{\epsilon P_T}{M-1}X_{4,4}} < \frac{\|\mathbf{h}\|^2}{\beta}|\Phi, \mathbf{h}, g_B\Big] \\
&= P\Big[X_4 < \left(\frac{\|\mathbf{h}\|^2}{\beta}d_{AE_e}^\alpha + \frac{\|\mathbf{h}\|^2}{\beta}\frac{\epsilon P_T y}{M-1}\right)|\Phi, \mathbf{h}, g_B\Big] \\
&= \int_0^\infty F_{X_4}\left(\frac{\|\mathbf{h}\|^2}{\beta}d_{AE_e}^\alpha + \frac{\|\mathbf{h}\|^2}{\beta}\frac{\epsilon P_T y}{M-1}\right) f_{X_{4,4}}(y)\mathrm{d}y \\
&= \int_0^\infty \left[1 - \exp\left\{-\left(\frac{\|\mathbf{h}\|^2}{\beta}d_{AE_e}^\alpha + \frac{\|\mathbf{h}\|^2}{\beta}\frac{\epsilon P_T y}{M-1}\right)\right\}\right] \\
&\quad \times f_{X_{4,4}}(y)\mathrm{d}y \\
&= 1 - \int_0^\infty \exp\left\{-\left(\frac{\|\mathbf{h}\|^2}{\beta}d_{AE_e}^\alpha + \frac{\|\mathbf{h}\|^2}{\beta}\frac{\epsilon P_T y}{M-1}\right)\right\} \\
&\quad \times \frac{y^{M-2}e^{-y}}{\Gamma(M-1)}\mathrm{d}y \\
&= 1 - \frac{e^{-\frac{\|\mathbf{h}\|^2}{\beta}d_{AE_e}^\alpha}}{\Gamma(M-1)}\int_0^\infty e^{-(1+\frac{\|\mathbf{h}\|^2}{\beta}\frac{\epsilon P_T}{M-1})y}y^{M-2}\mathrm{d}y \\
&= 1 - \frac{e^{-\frac{z}{\beta}\frac{d_{AE_e}^\alpha}{P_T}}}{(1+\frac{z}{\beta}\frac{\epsilon}{M-1})^{M-1}} \qquad (62) \\
&= 1 - \Omega(z; r, \theta), \qquad (63)
\end{aligned}$$

And then

$$\begin{aligned}
&\int_0^R \int_0^{2\pi} \Omega(z; r, \theta)d\theta r\mathrm{d}r \\
&= \frac{2\pi}{(1+\frac{\epsilon z}{\beta(M-1)})^{M-1}}\int_0^R e^{-\frac{zr^\alpha}{\beta P_T}}r\mathrm{d}r \\
&= \frac{2\pi\beta^{\frac{2}{\alpha}}}{\alpha(\|\mathbf{h}\|^2)^{\frac{2}{\alpha}}(1+\frac{\epsilon P_T}{M-1}\frac{\|\mathbf{h}\|^2}{\beta})^{M-1}}\int_0^{\frac{R^\alpha\|\mathbf{h}\|^2}{\beta}} e^{-y}y^{\frac{2}{\alpha}-1}y\mathrm{d}y \\
&= \frac{2\pi\beta^{\frac{2}{\alpha}}}{\alpha(\|\mathbf{h}\|^2)^{\frac{2}{\alpha}}(1+\frac{\epsilon P_T}{M-1}\frac{\|\mathbf{h}\|^2}{\beta})^{M-1}}\gamma\left(\frac{2}{\alpha}, \frac{R^\alpha\|\mathbf{h}\|^2}{\beta}\right). \qquad (64)
\end{aligned}$$

which is (29).

Appendix H
Proof of (30)

$$\begin{aligned}
&P[S_{AB_n} > R_s|d_{AB_n}, \Phi_E] \\
&= P[\max_{e\in\Phi_E} SNR_{AE_e} < \frac{SNR_{AB_n}}{\beta} + (\frac{1}{\beta} - 1)] \\
&= P[\max_{e\in\Phi_E} \frac{(1-\epsilon)P_T X_4}{d_{AE_e}^\alpha + \frac{\epsilon P_T}{M-1}X_{4,4}} < \frac{(1-\epsilon)P_T X_{2,n}}{\beta d_{AB_n}^\alpha} + (\frac{1}{\beta} - 1)] \\
&\approx P[\max_{e\in\Phi_E} \frac{X_4}{d_{AE_e}^\alpha + \frac{\epsilon P_T}{M-1}X_{4,4}} < \frac{X_{2,n}}{\beta d_{AB_n}^\alpha}] \quad \text{(for large } P_T\text{)}
\end{aligned}$$

And then

$$\begin{aligned}
&P[\max_{e\in\Phi_E} \frac{X_4}{d_{AE_e}^\alpha + \frac{\epsilon P_T}{M-1}X_{4,4}} < \frac{X_{2,n}}{\beta d_{AB_n}^\alpha}] \\
&= \prod_{e\in\Phi_E} P[\frac{X_4}{X_{2,n}} < \frac{d_{AE_e}^\alpha + \frac{\epsilon P_T}{M-1}X_{4,4}}{\beta d_{AB_n}^\alpha}] \\
&= \prod_{e\in\Phi_E} \int_0^\infty f_{X_{4,4}}(x)F_{\frac{X_4}{X_{2,n}}}\left(\frac{d_{AE_e}^\alpha + \frac{\epsilon P_T}{M-1}X_{4,4}}{\beta d_{AB_n}^\alpha}\right)\mathrm{d}x \\
&= \prod_{e\in\Phi_E} \int_0^\infty f_{X_{4,4}}(x)\left[1 - \left(1 + \frac{d_{AE_e}^\alpha + \frac{\epsilon P_T}{M-1}X_{4,4}}{\beta d_{AB_n}^\alpha}\right)^{-M}\right]\mathrm{d}x \\
&= \prod_{e\in\Phi_E} \left(1 - \int_0^\infty f_{X_{4,4}}(x)\left(1 + \frac{d_{AE_e}^\alpha + \frac{\epsilon P_T}{M-1}x}{\beta d_{AB_n}^\alpha}\right)^{-M}\right)
\end{aligned}$$

$$= \prod_{e\in\Phi_E} \Big(1 - \frac{1}{(\frac{\epsilon P_T}{(M-1)\beta d_{AB_n}^{\alpha}})^M} U(M,2,\frac{(M-1)\beta d_{AB_n}^{\alpha}}{\epsilon P_T} + \frac{(M-1)d_{AE_e}^{\alpha}}{\epsilon P_T})\Big), \quad (65)$$

where U denotes the confluent hypergeometric function of the second kind [42]. After applying Campbell's theorem [38] and setting $d_{AE_e} = r$, we have

$$P[S_{AB} > R_s | d_{AB_n}] = \exp\Big(-2\pi\rho_E (\frac{(M-1)\beta d_{AB_n}^{\alpha}}{\epsilon P_T})^M \times \int_0^{\infty} U(M,2,\frac{(M-1)\beta d_{AB_n}^{\alpha}}{\epsilon P_T} + \frac{(M-1)r^{\alpha}}{\epsilon P_T}) r \mathrm{d}r\Big). \quad (66)$$

Further simplification can be done by using proof as shown in subsection VI-B:

$$\Big(\frac{(M-1)\beta d_{AB_n}^{\alpha}}{\epsilon P_T}\Big)^M \int_0^{\infty} U(M,2,\frac{(M-1)\beta d_{AB_n}^{\alpha}}{\epsilon P_T} + \frac{(M-1)r^{\alpha}}{\epsilon P_T}) r\mathrm{d}r = \frac{1}{\alpha}\frac{(\beta d_{AB_n}^{\alpha})^M B(M-\frac{2}{\alpha},\frac{2}{\alpha})}{(\frac{\epsilon P_T}{M-1})^{M-\frac{2}{\alpha}}} U(M-\frac{2}{\alpha},2-\frac{2}{\alpha},\frac{(M-1)\beta d_{AB_n}^{\alpha}}{\epsilon P_T}). \quad (67)$$

B. Proof of (67)

Using the change of variables $c = \frac{(M-1)\beta d_{AB_n}^{\alpha}}{\epsilon P_T}$, we can write

$$(\frac{(M-1)\beta d_{AB_n}^{\alpha}}{\epsilon P_T})^M \int_0^{\infty} U(M,2,\frac{(M-1)\beta d_{AB_n}^{\alpha}}{\epsilon P_T} + \frac{(M-1)r^{\alpha}}{\epsilon P_T}) r\mathrm{d}r = \frac{c^M}{\Gamma(M)} \int_{r=0}^{\infty}\int_{t=0}^{\infty} e^{-(c+\frac{(M-1)r^{\alpha}}{\epsilon P_T})t} t^{M-1}(1+t)^{2-M-1}\mathrm{d}t r\mathrm{d}r = \frac{c^M}{\Gamma(M)} \int_{t=0}^{\infty}\Big(e^{-ct}t^{M-1}(1+t)^{1-M}\int_{r=0}^{\infty} e^{-\frac{(M-1)r^{\alpha}}{\epsilon P_T}t} r\mathrm{d}r\Big)\mathrm{d}t.$$

Using another change of variables $x = \frac{(M-1)r^{\alpha}}{\epsilon P_T}t$, the above becomes

$$\frac{(\frac{\epsilon P_T}{M-1})^{\frac{2}{\alpha}} c^M \Gamma(\frac{2}{\alpha})}{\alpha\Gamma(M)} \int_0^{\infty} e^{-ct} t^{M-\frac{2}{\alpha}-1} \times (1+t)^{2-\frac{2}{\alpha}-M+\frac{2}{\alpha}-1}\mathrm{d}t = \frac{(\frac{\epsilon P_T}{M-1})^{\frac{2}{\alpha}} c^M \Gamma(\frac{2}{\alpha})\Gamma(M-\frac{2}{\alpha})}{\alpha\Gamma(M)} \frac{1}{\Gamma(M-\frac{2}{\alpha})} \times \int_0^{\infty} e^{-ct} t^{M-\frac{2}{\alpha}-1}(1+t)^{2-\frac{2}{\alpha}-M+\frac{2}{\alpha}-1}\mathrm{d}t = \frac{(\frac{\epsilon P_T}{M-1})^{\frac{2}{\alpha}} c^M B(M-\frac{2}{\alpha},\frac{2}{\alpha})}{\alpha} \times U(M-\frac{2}{\alpha},2-\frac{2}{\alpha},\frac{(M-1)\beta d_{AB_n}^{\alpha}}{\epsilon P_T}). \quad (68)$$

APPENDIX I
PROOF OF (31)

When $\epsilon = 0$, we have

$$P[S_{AB_n} > R_s | d_{AB_n}, \Phi_E] = P[\max_{e\in\Phi_E} \frac{P_T X_4}{d_{AE_e}^{\alpha}} < \frac{P_T X_{2,n}}{\beta d_{AB_n}^{\alpha}} + \frac{1}{\beta} - 1] \approx P[\max_{e\in\Phi_E} \frac{X_4}{d_{AE_e}^{\alpha}} < \frac{X_{2,n}}{\beta d_{AB_n}^{\alpha}}] \quad \text{(for large } P_T\text{)} = \prod_{e\in\Phi_E} P[\frac{X_4}{X_{2,n}} < \frac{d_{AE_e}^{\alpha}}{\beta d_{AB_n}^{\alpha}}], \quad (69)$$

where $\frac{X_4}{X_{2,n}}$ follows an F-distribution, i.e., $f_{\frac{X_4}{X_{2,n}}}(x) = M(1+x)^{-(M+1)}$ and $F_{\frac{X_4}{X_{2,n}}}(x) = 1-(1+x)^{-M}$. Then,

$$P[S_{AB_n} > R_s | d_{AB_n}, \Phi_E] = \prod_{e\in\Phi_E} \Big(1-(1+\frac{d_{AE_e}^{\alpha}}{\beta d_{AB_n}^{\alpha}})^{-M}\Big). \quad (70)$$

After applying the Campbell's theorem [38] and setting $d_{AE_e} = r$ and $d_{AB_n} = x$, we have

$$P[S_{AB_n} > R_s | d_{AB_n}] = \exp\Big(-\frac{2}{\alpha}\pi\rho_E\beta^{\frac{2}{\alpha}} d_{AB_n}^2 \times B(M-\frac{2}{\alpha},\frac{2}{\alpha})\Big). \quad (71)$$

The computation of averaged SOP requires the PDF of the distance of the nth nearest user. The following lemma is known [35]:

Lemma 4: The PDF of d_{AB_n} is

$$f_{d_{AB_n}}(x) = \exp(-\rho_U\pi x^2)\frac{2\rho_U^n \pi^n x^{2n-1}}{\Gamma(n)}. \quad (72)$$

It now follows from this lemma and (71) that

$$P[S_{AB} > R_s] = \int_0^{\infty} \exp\Big(-\frac{2}{\alpha}\pi\rho_E\beta^{\frac{2}{\alpha}} x^2 B(M-\frac{2}{\alpha},\frac{2}{\alpha})\Big) \times \exp(-\rho_U\pi x^2)\frac{2\rho_U^n\pi^n x^{2n-1}}{\Gamma(n)}\mathrm{d}x = \frac{1}{\Big(1+\frac{\rho_E}{\rho_U}\frac{2}{\alpha}\beta^{\frac{2}{\alpha}} B(M-\frac{2}{\alpha},\frac{2}{\alpha})\Big)^n}.$$

APPENDIX J
PROOF OF (34)

By definition, we have

$$\mathcal{L}_{I_e}(s) = E_{\Phi}E_{I_e}\big[\exp(-s\sum_{e\in\Phi}\frac{|h_{A_{i^*}E_e}|^2}{\frac{d_{AE_e}^{\alpha}}{P_T} + \frac{d_{AE_e}^{\alpha}}{d_{BE_e}^{\alpha}} m X_2})\big] = E_{\Phi}\big[\prod_{e\in\Phi} E[\exp(-sH_e)]\big], \quad (73)$$

where $H_e = \frac{1}{f_e}\frac{|h_{A_{j^*}E_e}|^2}{\frac{d_{BE_e}^{\alpha}}{P_J} + X_2} = \frac{1}{f_e}\mathcal{X}_e$. From Lemma 1 or (18) with $M=1$, we know $f_{\mathcal{X}_e}(x_e) = e^{-\frac{d_{BE_e}^{\alpha}}{P_J}x_e}\Big(\frac{1}{(1+x_e)^2} + \frac{\frac{d_{BE_e}^{\alpha}}{P_J}}{1+x_e}\Big)$.

Then,

$$
\begin{aligned}
&E[e^{-sH_e}] \\
&= \int_0^\infty e^{-sh_e} f_{H_e}(h_e) dh_e = \int_0^\infty e^{-s\frac{x_e}{f_e}} f_{\mathcal{X}_e}(x_e) \mathrm{d}x_e \\
&= \int_0^\infty e^{-\frac{(s+\frac{d_{AE_e}^\alpha}{P_T})}{f_e} x_e} \left(\frac{1}{(1+x_e)^2} + \frac{d_{BE_e}^\alpha}{P_J} \frac{1}{(1+x_e)} \right) \mathrm{d}x_e \\
&= \int_0^\infty e^{-K(s)x_e} \left(\frac{1}{(1+x_e)^2} + (K(s) - \frac{s}{f_e}) \frac{1}{(1+x_e)} \right) \mathrm{d}x_e \\
&= \int_0^\infty \frac{e^{-K(s)x_e}}{(1+x_e)^2} \mathrm{d}x_e + (K(s) - \frac{s}{f_e}) \int_0^\infty \frac{e^{-K(s)x_e}}{(1+x_e)} \mathrm{d}x_e \\
&= 1 - e^{K(s)} K(s) \mathbf{E_1}(K(s)) + (K(s) - \frac{s}{f_e}) e^{K(s)} \mathbf{E_1}(K(s)) \\
&= 1 - \frac{s}{f_e} \mathbf{E_1}(K(s)) e^{K(s)}, \qquad (74)
\end{aligned}
$$

where $\mathbf{E_1}(a) = \int_0^\infty \frac{e^{-ax}}{1+x} \mathrm{d}x$ and $K(s) = \frac{s+\frac{d_{AE_e}^\alpha}{P_T}}{f_e}$. So we get:

$$
\begin{aligned}
\mathcal{L}_{I_e}(s) &= E_\Phi \Big[\prod_{e \in \Phi} E[\exp(-sH_e)] \Big] \\
&= E_\Phi \Big[\prod_{e \in \Phi} 1 - \frac{s}{f_e} \mathbf{E_1}(K(s)) e^{K(s)} \Big] \\
&= \exp \left[-\rho_E \int_0^R \int_0^{2\pi} \frac{s}{f_e} \mathbf{E_1}(K(s)) e^{K(s)} \mathrm{d}\theta r \mathrm{d}r \right]. \qquad (75)
\end{aligned}
$$

ACKNOWLEDGMENT

The views and conclusion contained in this document are those of the authors and should not be interpreted as representing the official policies, either expressed or implied, of the Army Research Office or the U.S. Government. The U.S. Government is authorized to reproduce and distribute reprints for Government purposes notwithstanding any copyright notation herein.

REFERENCES

[1] A. D. Wyner, "The wire-tap channel," *Bell Syst. Tech. J.*, vol. 54, no. 8, pp. 1355–1387, Oct. 1975.

[2] N. Yang, L. Wang, G. Geraci, M. Elkashlan, J. Yuan, and M. D. Renzo, "A safeguarding 5G wireless communication networks using physical layer security," *IEEE Commun. Mag.*, vol. 53, no. 4, pp. 20–27, Apr. 2015.

[3] E. Tekin and A. Yener, "The general Gaussian multiple access and twoway wire-tap channels: Achievable rates and cooperative jamming," *IEEE Trans. Inf. Theory*, vol. 54, pp. 2735–2751, Jun. 2008.

[4] H. Zhang, H. Xing, J. Cheng, A. Nallanathan, and V. C. M. Leung, "Secure resource allocation for OFDMA two-way relay wireless sensor networks without and with cooperative jamming," *IEEE Trans. Ind. Informat.*, vol. 12, no. 5, pp. 1714–1725, Oct. 2016.

[5] J. Zhang and M. C. Gursoy, "Relay beamforming strategies for physicallayer security," in *Proc. 44th Annu. Conf. Inf. Sci. Syst.*, Princeton, NJ, USA, Mar. 2010, pp. 1–6.

[6] H. Weingarten, T. Liu, S. Shamai, Y. Steinberg, and P. Viswanath, "The capacity region of the degraded multiple-input multiple-output compound broadcast channel," *IEEE Trans. Inf. Theory*, vol. 55, no. 11, pp. 5011–5023, Nov. 2009.

[7] L. Chen, Q. Zhu, W. Meng, and Y. Hua, "Fast power allocation for secure communication with full-duplex radio," *IEEE Trans. Signal Process.*, vol. 65, no. 14, pp. 3846–3861, Jul. 2017.

[8] G. Chen, Y. Gong, P. Xiao, and J. A. Chambers, "Dual antenna selection in secure cognitive radio networks," *IEEE Trans. Veh. Technol.*, vol. 65, no. 10, pp. 7993–8002, Oct. 2016.

[9] A. Khisti, G. Wornell, A. Wiesel, and Y. Eldar, "On the Gaussian MIMO wiretap channel," in *Proc. IEEE Int. Symp. Inf. Theory*, Nice, France, Jun. 2007, pp. 2471–2475.

[10] S. Goel and R. Negi, "Guaranteeing secrecy using artificial noise," *IEEE Trans. Wireless Commun.*, vol. 7, no. 6, pp. 2180–2189, Jun. 2008.

[11] Y. Huang, J. Wang, C. Zhong, T. Q. Duong, and G. K. Karagiannidis, "Secure transmission in cooperative relaying networks with multiple antennas," *IEEE Trans. Wireless Commun.*, vol. 15, no. 10, pp. 6843–6856, Oct. 2016.

[12] M. Yang, B. Zhang, Y. Huang, N. Yang, D. B. da Costa, and D. Guo, "Secrecy enhancement of multiuser MISO networks using OSTBC and artificial noise," *IEEE Trans. Veh. Technol.*, vol. 66, no. 12, pp. 11394–11398, Dec. 2017.

[13] M. Haenggi, "The secrecy graph and some of its properties," in *Proc. IEEE Int. Symp. Inf. Theory*, Toronto, ON, Canada, Jul. 2008, pp. 539–543.

[14] H. Wang, X. Zhou, and M. C. Reed, "Physical layer security in cellular networks: A stochastic geometry approach," *IEEE Trans. Wireless Commun.*, vol. 12, no. 6, pp. 2776–2787, Jun. 2013.

[15] X. Zhou, R. K. Ganti, and J. G. Andrews, "Secure wireless network connectivity with multi-antenna transmission," *IEEE Trans. Wireless Commun.*, vol. 10, no. 2, pp. 425–430, Feb. 2011.

[16] X. Zhang, X. Zhou, and M. R. McKay, "On the design of artificial-noise aided secure multi-antenna transmission in slow fading channels," *IEEE Trans. Veh. Technol.*, vol. 62, no. 5, pp. 2170–2181, Jun. 2013.

[17] T.-X. Zheng, H.-M. Wang, J. Yuan, D. Towsley, and M. H. Lee, "Multi-antenna transmission with artificial noise against randomly distributed eavesdroppers," *IEEE Trans. Commun.*, vol. 63, no. 11, pp. 4347–4362, Nov. 2015.

[18] L. Zhang, H. Zhang, D. Wu, and D. Yuan, "Improving physical layer security for MISO systems via using artificial noise," in *Proc. IEEE Global Commun. Conf. (GLOBECOM)*, Dec. 2015, pp. 1–6.

[19] T.-X. Zheng and H.-M. Wang, "Optimal power allocation for artificial noise under imperfect CSI against spatially random eavesdroppers," *IEEE Trans. Veh. Technol.*, vol. 65, no. 10, pp. 8812–8817, Oct. 2016.

[20] X. Zhang, X. Zhou, and M. R. McKay, "Enhancing secrecy with multi-antenna transmission in wireless ad hoc networks," *IEEE Trans. Inf. Forensics Security*, vol. 8, no. 11, pp. 1802–1814, Nov. 2013.

[21] M. Ghogho and A. Swami, "Physical-layer secrecy of MIMO communications in the presence of a Poisson random field of eavesdroppers," in *Proc. IEEE ICC*, Kyoto, Japan, Jun. 2011, pp. 1–5.

[22] X. Zhou, R. K. Ganti, J. G. Andrews, and A. Hjørungnes, "On the throughput cost of physical layer security in decentralized wireless networks," *IEEE Trans. Wireless Commun.*, vol. 10, no. 8, pp. 2764–2775, Aug. 2011.

[23] G. Geraci, S. Singh, J. G. Andrews, J. Yuan, and I. B. Collings, "Secrecy rates in broadcast channels with confidential messages and external eavesdroppers," *IEEE Trans. Wireless Commun.*, vol. 13, no. 5, pp. 2931–2943, May 2014.

[24] T.-X. Zheng, H.-M. Wang, and Q. Yin, "On transmission secrecy outage of a multi-antenna system with randomly located eavesdroppers," *IEEE Commun. Lett.*, vol. 18, no. 8, pp. 1299–1302, Aug. 2014.

[25] T. Riihonen, S. Werner, and R. Wichman, "Mitigation of loopback self-interference in full-duplex MIMO relays," *IEEE Trans. Signal Process.*, vol. 59, no. 12, pp. 5983–5993, Dec. 2011.

[26] Y. Hua, Y. Ma, A. Gholian, Y. Li, A. C. Cirik, and P. Liang, "Radio self-interference cancellation by transmit beamforming, all-analog cancellation and blind digital tuning," *Signal Process.*, vol. 108, pp. 322–340, Mar. 2015.

[27] T.-X. Zheng, H.-M. Wang, Q. Yang, and M. H. Lee, "Safeguarding decentralized wireless networks using full-duplex jamming receivers," *IEEE Trans. Wireless Commun.*, vol. 16, no. 1, pp. 278–292, Jan. 2017.

[28] T. Zhang, Y. Cai, Y. Huang, T. Q. Duong, and W. Yang, "Secure full-duplex spectrum-sharing wiretap networks with different antenna reception schemes," *IEEE Trans. Commun.*, vol. 65, no. 1, pp. 335–346, Jan. 2017.

[29] Y. Hua, Q. Zhu, and R. Sohrabi, "Fundamental properties of full-duplex radio for secure wireless communications," 2017, *arXiv:1711.10001*. [Online]. Available: http://arxiv.org/abs/1711.10001

[30] Y. Hua, "Advanced properties of full-duplex radio for securing wireless network," *IEEE Trans. Signal Process.*, vol. 67, no. 1, pp. 120–135, Jan. 2019.

[31] R. Sohrabi, Q. Zhu, and Y. Hua, "Secrecy analyses of a full-duplex MIMOME network," *IEEE Trans. Signal Process.*, vol. 67, no. 23, pp. 5968–5982, Dec. 2019.

[32] M. Xie and T.-M. Lok, "Antenna selection in RF-chain-limited MIMO interference networks under interference alignment," *IEEE Trans. Veh. Technol.*, vol. 66, no. 5, pp. 3856–3870, May 2017.
[33] G. Chen, J. P. Coon, and M. Di Renzo, "Secrecy outage analysis for downlink transmissions in the presence of randomly located eavesdroppers," *IEEE Trans. Inf. Forensics Security*, vol. 12, no. 5, pp. 1195–1206, May 2017.
[34] I. Zabir, A. Maksud, B. M. Sadler, and Y. Hua, "Secure downlink transmission to full-duplex user against randomly located eavesdroppers," in *Proc. IEEE Global Commun. Conf. (GLOBECOM)*, Waikoloa, HI, USA, Dec. 2019, pp. 1–6.
[35] G. Chen and J. P. Coon, "Secrecy outage analysis in random wireless networks with antenna selection and user ordering," *IEEE Wireless Commun. Lett.*, vol. 6, no. 3, pp. 334–337, Jun. 2017.
[36] Y. Hua, P. Liang, Y. Ma, A. C. Cirik, and Q. Gao, "A method for broadband full-duplex MIMO radio," *IEEE Signal Process. Lett.*, vol. 19, no. 12, pp. 793–796, Dec. 2012.
[37] P. B. Patnaik, "The non-central χ^2- and F-distribution and their applications," *Biometrika*, vol. 36, nos. 1–2, pp. 202–232, Jun. 1949.
[38] R. L. Streit, *The Poisson Point Process*. Boston, MA, USA: Springer, 2010.
[39] Y. Ju, H.-M. Wang, T.-X. Zheng, Q. Yin, and M. H. Lee, "Safeguarding millimeter wave communications against randomly located eavesdroppers," *IEEE Trans. Wireless Commun.*, vol. 17, no. 4, pp. 2675–2689, Apr. 2018.
[40] C. Wang and H.-M. Wang, "Physical layer security in millimeter wave cellular networks," *IEEE Trans. Wireless Commun.*, vol. 15, no. 8, pp. 5569–5585, Aug. 2016.
[41] T. Bai and R. W. Heath, Jr., "Coverage and rate analysis for millimeter-wave cellular networks," *IEEE Trans. Wireless Commun.*, vol. 14, no. 2, pp. 1100–1114, Feb. 2015.
[42] L. C. Andrews, *Special Functions of Mathematics for Engineers*. Bellingham, WA, USA: SPIE, 1998, ch. 10.
[43] L. Bostock, S. Chandler, and F. S. Chandler, *Pure Mathematics 2*. Cheltenham, U.K.: Nelson Thornes, 1979.
[44] S. Sanayei and A. Nosratinia, "Antenna selection in MIMO Systems," *IEEE Commun. Mag.*, vol. 42, no. 10, pp. 68–73, Oct. 2004.
[45] L. Dritsoula, Z. Wang, H. R. Sadjadpour, and J. J. Garcia-Luna-Aceves, "Antenna selection for opportunistic interference management in MIMO broadcast channels," in *Proc. IEEE 11th Int. Workshop Signal Process. Adv. Wireless Commun. (SPAWC)*, Jun. 2010, pp. 1–5.
[46] Y. Gao and T. Kaiser, "Antenna selection in massive MIMO systems: Full-array selection or subarray selection?" in *Proc. IEEE Sensor Array Multichannel Signal Process. Workshop (SAM)*, Jul. 2016, pp. 1–5.
[47] H. Alves, R. D. Souza, M. Debbah, and M. Bennis, "Performance of transmit antenna selection physical layer security schemes," *IEEE Signal Process. Lett.*, vol. 19, no. 6, pp. 372–375, Jun. 2012.

Ishmam Zabir (Graduate Student Member, IEEE) received the B.Eng. degree in electrical and electronics engineering from the Bangladesh University of Engineering and Technology, Bangladesh, in 2015. He is currently pursuing the Ph.D. degree in electrical and computer engineering with the University of California Riverside, Riverside, CA, USA. His research interests include physical-layer security in wireless network, full-duplex radio, resource allocation in distributed networks, and stochastic geometry.

Ahmed Maksud (Student Member, IEEE) received the B.Sc. degree in electrical and electronics engineering from the Bangladesh University of Engineering and Technology, Dhaka, Bangladesh, in 2017. He is currently pursuing the Ph.D. degree in electrical and computer engineering with the University of California at Riverside, Riverside, CA, USA. His research interests include wireless communication, wireless networks security, and full-duplex radio.

Gaojie Chen (Senior Member, IEEE) received the B.Eng. and B.Ec. degrees in electrical information engineering and international economics and trade from Northwest University, China, in 2006, and the M.Sc. (Hons.) and Ph.D. degrees in electrical and electronic engineering from Loughborough University, Loughborough, U.K., in 2008 and 2012, respectively. He is currently a Lecturer with the School of Engineering, University of Leicester, U.K. He serves as an Associate Editor for the IEEE COMMUNICATIONS LETTERS, IEEE WIRELESS COMMUNICATIONS LETTERS, IEEE JOURNAL ON SELECTED AREAS IN COMMUNICATIONS - *Machine Learning in Communications and Networks* and *Electronics Letters* (IET).

Brian M. Sadler (Life Fellow, IEEE) received the B.S. and M.S. degrees from the University of Maryland, College Park, MD, USA, and the Ph.D. degree from the University of Virginia, Charlottesville, VA, USA, all in electrical engineering. He has been an IEEE Communications Society Distinguished Lecturer since 2020, was an IEEE Signal Processing Society Distinguished Lecturer from 2017 to 2018, and the General Co-Chair of IEEE GlobalSIP'16. He is currently the U.S. Army Senior Scientist for Intelligent Systems, and a fellow of the Army Research Laboratory (ARL), Adelphi, MD, USA. He has more than 400 publications in these areas with 17,000 citations and H-index of 56. His research interests include information science, and networked collaborative autonomous intelligent systems. He received Best Paper awards from the IEEE Signal Processing Society in 2006 and 2010, several ARL and Army R/D awards, and the 2008 Outstanding Invention of the Year Award from the University of Maryland. He has been an Associate Editor of the IEEE TRANSACTIONS ON SIGNAL PROCESSING, IEEE SIGNAL PROCESSING LETTERS, and *EURASIP Signal Processing*, and a Guest Editor for several journals, including the IEEE JOURNAL OF SELECTED TOPICS IN SIGNAL PROCESSING (JSTSP), the IEEE JOURNAL ON SELECTED AREAS IN COMMUNICATIONS (JSAC), IEEE TRANSACTIONS ON ROBOTICS (T-RO), the *IEEE SP Magazine*, *Autonomous Robots*, and *The International Journal of Robotics Research*.

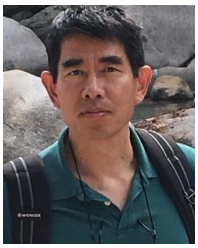

Yingbo Hua (Fellow, IEEE) received the B.S. degree from Southeast University, Nanjing, China, in 1982, and the Ph.D. degree from Syracuse University, NY, USA, in 1988. He joined the faculty of the University of Melbourne, Melbourne, VIC, Australia, in 1990, where he was promoted to a Reader and an Associate Professor, in 1996. He moved to the University of California, Riverside, CA, USA, as a Full Professor, in 2001, where he advanced to a Senior Full Professor in 2009 and a Professor IX in 2019. He has published more than 340 articles in signal processing, wireless communications, and sensor networks, with citations more than 13520 and H-Index 55. He has been a fellow of AAAS since 2011. Since 1994, he has been serving in a number of editorial and leadership roles for IEEE TRANSACTIONS ON SIGNAL PROCESSING, IEEE SIGNAL PROCESSING LETTERS, *Signal Processing*, *IEEE Signal Processing Magazine*, IEEE JOURNAL OF SELECTED AREAS IN COMMUNICATIONS, IEEE WIRELESS COMMUNICATIONS LETTERS, and IEEE TRANSACTIONS ON SIGNAL AND INFORMATION PROCESSING OVER NETWORKS. He was the General Co-Chair of IEEE ChinaSIP'2015, and the Lead Chair of IEEE GlobalSIP'2018 Symposium on Signal Processing for Wireless Network Security. He is currently the Chair of the Steering Committee for IEEE WIRELESS COMMUNICATIONS LETTERS.